NATIONAL ADVISORY COMMITTEE FOR AERONAUTICS

TECHNICAL MEMORANDUM 1279

TWO-DIMENSIONAL SYMMETRICAL INLETS WITH EXTERNAL COMPRESSION

By P. Ruden

Translation of ZWB Forschungsbericht Nr. 1209, April 15, 1940

Washington
March 1950

NATIONAL ADVISORY COMMITTEE FOR AERONAUTICS

TECHNICAL MEMORANDUM 1279

TWO-DIMENSIONAL SYMMETRICAL INLETS WITH EXTERNAL COMPRESSION*

By P. Ruden

FOREWORD BY REVIEWER

The accompanying report is considered significant in that it gives the only analytical development of maximum-critical-speed air inlets. Wind-tunnel tests of two-dimensional[1] and rotationally symmetrical[2] inlets built to the ordinates derived herein were also made by Ruden. In all cases the predicted flat pressure distributions were obtained at the predicted minimum inlet-velocity ratios.

It is interesting that at nearly the same time the development of nearly identical high-critical-speed inlets was proceeding experimentally in the United States. This development was summarized and set up for design application by Baals, Smith, and Wright[3].

To those reading the accompanying report, the other three reports listed in the footnotes here are recommended as valuable additional material. With their aid, an exceptionally good picture of the theory, development, and application of air inlets may be obtained.

J. Ford Johnston
Langley Aeronautical Laboratory

---

*"Ebne symmetrische Fangdiffusoren." Zentrale für wissenschaftliches Berichtswesen über Luftfahrtforschung (ZWB) Berlin-Adlershof, Forschungsbericht Nr. 1209, April 15, 1940.

[1]Ruden, P.: Windkanalmessungen an ebnen, symmetrischen Fangdiffusoren (Wind-Tunnel Tests of Two-Dimensional Symmetrical External Compression Inlets). Forschungsbericht Nr. 1325, Dec. 1940.

[2]Ruden, P.: Windkanalmessungen an einem rotationssymmetrischen Fangdiffusor (Wind-Tunnel Tests of a Rotationally Symmetrical External-Compression Inlet). Forschungsbericht Nr. 1427/1, March 1941.

[3]Baals, D. D., Smith, N. F., and Wright, J. B.: The Development and Application of High-Critical-Speed Nose Inlets. NACA Rep. 920, 1948.

Abstract: The purpose of inlets like, for instance, those of air-cooled radiators and scoops is to take a certain air quantity out of the free stream and to partly convert the free-stream velocity into pressure. In the extreme case this pressure conversion may occur either entirely in the interior of the inlet (inlet with internal compression) or entirely in the free stream ahead of the inlet (inlet with external compression). In this report a theory for two-dimensional inlets with external compression is developed and illustrated by numerical examples. Intermediary forms between inlets with internal and external compression which can be derived from the latter are briefly discussed.

The report is meant chiefly for the theoretical aerodynamicist; however, sections I and VII apply directly to the designer.

Outline:

SYMBOLS

w_∞ free-stream velocity (real)

w_i final velocity in the interior of the inlet (real)

u velocity component, parallel to the free-stream velocity

v	velocity component, perpendicular to the free-stream velocity
$w = u - iv$	complex velocity
p	local pressure
p_i	final pressure in the interior of the inlet
$q = \left(\frac{\rho}{2}\right)w_\infty^2$	free-stream dynamic pressure
S	nose thrust
d	wall thickness of the inlet
h	half height of the inlet opening
$z = x + iy$	coordinate of the flow plane

I. DEFINITION OF CONCEPTS OF INLETS WITH EXTERNAL AND INTERNAL COMPRESSION. STATEMENT OF THE PROBLEM.

In many aerodynamic questions of airplane construction one has to deal with the following problem: A certain air quantity is to be taken from the free stream and, mostly with conversion of velocity into pressure, to be conveyed to propulsion units or airplane accessories. A typical example, largely discussed lately, is the radiator with cowling. It shows that the aerodynamically faultless design of the inlet is rendered difficult, above all, by the requirement that the pressure conversion expressed in the ratio mean velocity in the interior of the inlet (w_i) to the flight velocity (w_∞) be made adjustable to a high extent. It is true that this can be accomplished fundamentally only by suitable measures at the outlet of the device which is here of no further interest; however, for the following discussion the empirical fact is important that the excess velocity either - for small w_i/w_∞ - at the outer, or - if w_i/w_∞ almost reaches the amount 1 - at the inner nose contour easily becomes so large that flow separation and vortex formation occur. In the first case the drag of the inlet undergoes a sudden increase, in the second the diffuser efficiency undergoes a considerable deterioration. Evidently, excess velocities of such an order of magnitude must be avoided. For fast airplanes, however, even this limit frequently lies much too high: always, if the local Mach number should exceed, for instance, a value of about 0.95.

If the range of regulation for w_1/w_∞ is not large, the aerodynamic problem may be solved by making the entrance opening of the inlet (approximately in accordance with the inverse ratio of the velocity retardation) smaller than the inner cross section. Inlets of this kind shall be called "inlets with internal compression." (See fig. 1.) In their ideal form the walls of these inlets are simply "frozen" streamlines which are obtained when, in a flow field with constant velocity everywhere, a stagnation is made to occur by means of a screen or the like. In these devices, the pressure conversion takes place more or less completely in the interior of the inlet, with an efficiency which is unavoidably smaller than 1. If w_1/w_∞ becomes noticeably larger than the velocity ratio to which the opening ratio was adjusted, the flow in the inlet tends (even for rounded noses) toward separation; hence the diffuser efficiency generally deteriorates considerably. This disadvantage can be prevented by making the opening ratio of the inlet adjustable by means of a suitable mechanism. On the other hand, it is probably always possible to adhere, for inlets with internal compression of this kind, to the permissible maximum velocity on the external contour.

The "inlets with external compression" are characterized by the entrance cross section being equal to the maximum cross section of the inlet. Here the pressure conversion is shifted entirely to the free stream (fig. 2) and is, therefore, for all velocity ratios between 0 and 1 completely free of loss. However, the flow along the external contour of the inlet is endangered: the maximum velocity existing there can be kept within permissible limits only by careful shaping of the outer nose contours and by selection of a sufficient wall thickness. However, once this is attained for the smallest velocity ratio w_1/w_∞, the inlet with external compression operates faultlessly as well for any larger velocity ratio up to $w_1/w_\infty = 1$ and even slightly beyond this value; thus an adjustment mechanism of the inlet may be omitted.

Between inlets with purely external and purely internal compression there exists an abundance of intermediary forms; these originate from the inlet with internal compression by adding thickness to the hollow inner wall, from the inlet with external compression by reducing the wall thickness from the inside. The latter forms will be discussed in somewhat more detail in section VII. The intermediary forms may be of great practical importance; they are, however, hardly suitable for theoretical treatment, and their investigation is mostly limited to wind-tunnel tests.

In order to reexamine whether the required wall thicknesses of the inlets with external compression lie within boundaries attainable in practice, and to create, at the same time, a basis for the calculation of such inlets, a theory of two-dimensional inlets with external compression is developed below. A few idealizations are necessary: first, limitation to incompressible flow; second, neglect of all boundary-layer effects

(frictionless fluid); third, elongation of the inlet in flow direction to infinity. (See fig. 3.) The first two simplifications need no explanation as necessary requirements. About the third, it is to be noted that all essential phenomena take place around the entrance of the inlet with external compression and that an outlet of different shape does not exert a strong influence on the entrance flow, if the device is sufficiently long. However, possible deviations of the theory from actual conditions can and must be determined by additional investigations, chiefly, probably, of experimental character.

The present report deals with symmetrical inlets with external compression only, where the two walls are of identical form. Unsymmetrical inlets with external compression are considered only inasmuch as they can be derived from the symmetrical ones.

The problem of the three-dimensional design of inlets with external compression remains at first unsolved; however, the two-dimensional theory - exact under the given conditions - permits already so much insight into the essential properties of the inlet with external compression that one may hope, with the aid of the knowledge attained there, to be able to cope particularly with the three-dimensional inlet with external compression, since the excess velocity at the outer nose contour must be smaller in the three-dimensional than in the two-dimensional case due to the greater possibility for flow divergence around the body.

II. THE HODOGRAPH METHOD FOR PRODUCTION OF TWO-DIMENSIONAL-FLOW PATTERNS.

The hodograph method allows a relatively simple introduction into the theory of inlets with external compression. A detailed description of this method is to be found in the textbook by Prandtl-Tietjens. However, a brief compilation of its most important characteristics will be useful, particularly for the reason that thus a few view points of significance for the following can be specially emphasized.

If z is assumed to be the complex variable of the flow plane, $F(z)$ the complex flow potential,

$$w = f(z) = \frac{dF}{dz} = \frac{dF}{dw}\frac{dw}{dz} \tag{1}$$

is the so-called complex velocity which is related to the components u and v of the actual velocity by the equation

The analytical function $w = f(z)$ may be used for mapping the z-plane onto a complex w-plane. Thereby the flow pattern in the z-plane is mapped into the so-called hodograph flow: an arbitrary point of the z-plane is mapped precisely into the point which corresponds to its complex velocity w.

This fact makes it possible to give a qualitative presentation of the hodograph flow when there exists a qualitative presentation of the flow in the z-plane, or if one can procure in any other way a sufficient amount of data on magnitude and direction of the local flow velocities of the z-plane. At first, not much seems to be gained hereby. However, it is an empirical fact that the complex potential of the hodograph flow is sometimes simpler than the flow potential of the z-plane. In such cases it is mostly sufficient to build up the hodograph flow from a few of the simplest singularities which may be taken from the qualitative presentation of the hodograph flow. Where these singularities are no longer sufficient, one can proceed by analogy.

If $F(w)$, the complex potential of the hodograph flow, can be given, first, an exact presentation of the hodograph flow may be drawn and, by converse mapping of the w-plane on to the z-plane, also the flow pattern of the z-plane. This mapping is achieved, according to equation (1), by

$$z = \int \frac{dF}{w} + \text{const} = \int \frac{dF}{dw}\frac{dw}{w} + \text{const} \qquad (2)$$

If the velocity of the z-plane flow is required to be everywhere finite, the hodograph flow must necessarily be limited by a closed curve which may assume rather arbitrary shape. In the following discussion, however, only circles are admitted as boundaries so that the selection of the actually possible forms of inlets with external compression is definitely limited. By mapping the hodograph circle onto other simply connected regions, the theory developed here may be generalized to a great extent.

Due to the properties of the conformal mapping, the circular boundary of the hodograph must be mapped into boundary sections of the z-plane flow. Further boundary curves are (as will be shown later) represented by slits protruding into the interior of the hodograph circle. If the flow outside of the walls of the inlet with external compression is to be free from singularities, the interior of the hodograph circle (with exception of the slits) also must be free from singularities; otherwise the mapping performed by equation (2) would transplant these singularities into the z-plane.

Stagnation points of the z-plane flow situated in the finite domain require special attention. They are defined by $w = 0$ and the corresponding z is, according to equation (2), finite only when simulta-

neously dF/dw disappears. In such cases one must, therefore, make sure that the hodograph flow, the complex velocity of which is represented by dF/dw, has a stagnation point at the zero point of the w-plane.

For the external-compression inlet without special installations, the hodograph flow must not have any further stagnation points in the interior of the hodograph, apart from the aforementioned stagnation point. This follows directly from equation (1): $w = f(z)$ is in this case outside of the walls of the inlet with external compression an analytical function free from singularities. The derivative dw/dz exists and is everywhere finite in this domain. Since, however, according to presupposition $w \neq 0$ therein, it must also follow from equation (1) that $dF/dw \neq 0$.

For the boundary curves this conclusion is no longer valid, since on them dw/dz may become infinitely large. One can easily see, however, that here further stagnation points of the hodograph flow are admissible only at reentrant corners; that is, only such stagnation points may be added in the neighborhood of which the flow direction does not change, if one travels along the corresponding streamline in a certain direction. Otherwise convergence or mutual penetration of the boundary lines in the z-plane could occur; both possibilities shall be excluded below.

III. CONSTRUCTION OF THE SIMPLEST SYMMETRICAL HODOGRAPH.

According to the directions for the construction of a hodograph, one first designs a qualitative stream line pattern of the symmetrical inlet with external compression. (See fig. 4(a).) In order to obtain the mapping of a streamline in the w-plane, one draws - starting from the zero point of the w-plane - the complex velocity vectors of the streamline for a sufficient number of points; one then connects the heads of these vectors and determines simultaneously a direction of travel corresponding to the sequence of vectors in the z-plane. The streamlines $A_\infty, A_o, A_1/A_o, A_2$ for instance are represented in the w-plane in the train of lines $1, 0, w_{max}, 1/0, w_i$ (See fig. 4(b).) It is assumed that the magnitude of the velocity is constant along the entire nose contour (semicircle in the w-plane) and that the velocity at infinity equals 1. If the w-plane is supplemented by the mapping of further streamline patterns, the mapping of the hodograph (fig. 5) is obtained. The streamlines of the hodograph flow all start from $w = 1$ and end partly at $w = w_i$, mostly, however, at their starting point $w = 1$. Hence one concludes that a source and a doublet must be present at $w = 1$, a sink at $w = w_i$. For reasons of continuity, the sink is of the same strength as the source.

Since the circle H with the radius R is a streamline, the expression (35) of the appendix is to be set up as complex partial potential for source and sink, the expression (36) as doublet potential. The total potential is

$$F(w) = \frac{Q}{2\pi} \ln \frac{(w - 1)\left(w - R^2\right)}{\left(w - w_i\right)\left(w - \frac{R^2}{w_i}\right)} + \frac{M}{2\pi}\left[\frac{1}{w - 1} - \frac{*R^2}{w - R^2}\right] \tag{3}$$

Hence follows with $M = fQ$ the complex velocity of the hodograph flow

$$\frac{dF}{dw} = \frac{Q}{2\pi}\left[\frac{1}{w - 1} - \frac{1}{w - w_i} + \frac{1}{w - R^2} - \frac{1}{w - \frac{R^2}{w_i}} - f\left\{\frac{1}{(w - 1)^2} - \frac{R^2}{\left(w - R^2\right)2}\right\}\right] \tag{4}$$

According to section II, the point $w = 0$ must be a stagnation point of the hodograph flow, that is, equation (4) must disappear at this point; thus

$$f = \frac{R^2\left(\frac{1}{w_i} - 1\right) - \left(1 - w_i\right)}{R^2 - 1} \tag{5}$$

If one introduces $w = w_1 + iw_2$ into equation (3), $F(w) = \varphi + i\psi$ may be readily divided into its real and its imaginary part. The imaginary part is the stream function of the hodograph flow:

$$\psi = \frac{Q}{2\pi}\left[\text{arc tan}\,\frac{w_2}{w_1 - 1} - \text{arc tan}\,\frac{w_2}{w_1 - w_i} + \text{arc tan}\,\frac{w_2}{w_1 - R^2}\right.$$

$$\left. - \text{arc tan}\,\frac{w_2}{w_1 - \frac{R^2}{w_i}} - fw_2\left\{\frac{1}{\left(w_1 - 1\right)^2 + w_2^2} - \frac{R^2}{\left(w_1 - R^2\right)^2 + w_2^2}\right\}\right] \tag{6}$$

*Reviewer's note: This value was erroneously given as $\frac{R}{w - R^2}$ in the original German version of the report.

The lines ψ = const. are the streamlines of the symmetrical hodograph. (See for instance, fig. 5.) For their numerical calculation one starts from a prescribed w_2 (or w_1) and varies w_1 (or w_2). One plots the values ψ thus obtained against w_1 (or w_2) and takes for ψ = const. the w_1 (or w_2) corresponding to the prescribed w_2 (or w_1). It is practical to select as streamline constant the value π/n (n integral), because $\psi = 0$ corresponds to the stagnation point streamlines and the contours of the inlet with external compression, $\psi = \pi$ to the symmetry streamline.

IV. CALCULATION OF THE SIMPLEST SYMMETRICAL INLETS WITH EXTERNAL COMPRESSION WITH CONSTANT VELOCITY ALONG THE NOSE CONTOUR.

With equation (4) one enters into equation (2) and obtains after simple calculation:

$$z = \frac{Q}{2\pi}\left[(1+f)\ln(w-1) - \frac{1}{w_i}\ln(w-w_i) + \frac{1-f}{R^2}\ln(w-R^2)\right.$$
$$- \frac{w_i}{R^2}\ln\left(w - \frac{R^2}{w_i}\right) + \frac{f}{w-1} - \frac{f}{w-R^2} + \frac{\ln w}{R^2}\left\{R^2\left(\frac{1}{w_i} - 1\right)\right.$$
$$\left.\left. - (1 - w_i) - f\left(R^2 - 1\right)\right\}\right] + \text{const}$$

Because of (5), the factor of $\ln w$ disappears. If, moreover, the arbitrary constant is equated to $x_o - ih$ with

$$x_o = \frac{Q}{2\pi R^2}\left[\left(\frac{R^2}{w_i} - w_i\right)\ln w_i + 2\left(f + w_i - 1\right)\ln R + f\left(R^2 - 1\right)\right] \tag{7}$$

then

$$z = \frac{Q}{2\pi}\left[(1+f)\ln(w-1) - \frac{1}{w_i}\ln(w-w_i) + \frac{1-f}{R^2}\ln(w-R^2)\right.$$
$$\left. - \frac{w_i}{R^2}\ln\left(w - \frac{R^2}{w_i}\right) + \frac{f}{w-1} - \frac{f}{w-R^2}\right] + x_o - ih \tag{8}$$

is the analytical function which performs the mapping of the hodograph onto the z-plane. The constant is selected in such a manner that the real axis coincides with the symmetry line of the inlet with external compression and the imaginary axis of the z-plane goes through the two stagnation points.

The following symbols are introduced (fig. 6):

$$\left.\begin{aligned}
&w = w_1 + iw_2 \\
&w - w_i = l_1 e^{i\delta_1}, \quad l_1 = \sqrt{(w_1 - w_i)^2 + w_2^2}, \quad \delta_1 = \arctan \frac{w_2}{w_1 - w_i} \\
&w - 1 = l_2 e^{i\delta_2}, \quad l_2 = \sqrt{(w_1 - 1)^2 + w_2^2}, \quad \delta_2 = \arctan \frac{w_2}{w_1 - 1} \\
&w - R^2 = l_3 e^{i\delta_3}, \quad l_3 = \sqrt{(w_1 - R^2)^2 + w_2^2}, \quad \delta_3 = \arctan \frac{w_2}{w_1 - R^2} \\
&w - \frac{R^2}{w_i} = l_4 e^{i\delta_4}, \quad l_4 = \sqrt{\left(w_1 - \frac{R^2}{w_i}\right)^2 + w_2^2}, \quad \delta_4 = \arctan \frac{w_2}{w_1 - \frac{R^2}{w_i}}
\end{aligned}\right\} \quad (9)$$

Now equation (8) may be divided into its real and its imaginary parts

$$\left.\begin{aligned}
x = \frac{Q}{2\pi}\Bigg[&(1 + f)\ln l_2 - \frac{1}{w_i}\ln l_1 + \frac{1 - f}{R^2}\ln l_3 \\
&- \frac{w_i}{R^2}\ln l_4 + \frac{f}{l_2}\cos\delta_2 - \frac{f}{l_3}\cos\delta_3\Bigg] + x_o \\
y = \frac{Q}{2\pi}\Bigg[&(1 + f)\delta_2 - \frac{\delta_1}{w_i} + \frac{1 - f}{R^2}\delta_3 - \frac{w_i}{R^2}\delta_4 \\
&- \frac{f}{l_2}\sin\delta_2 + \frac{f}{l_3}\sin\delta_3\Bigg] - h
\end{aligned}\right\} \quad (10)$$

With these two equations and with equation (7) all streamlines of the symmetrical inlet with external compression can be calculated point by point from the streamlines of the hodograph. The quantities appearing in equation (10) l_v and δ_v are either determined according to the formulas (9) or taken from figure 6.

Due to the multivaluedness of the angles δ_v, which for the time being are determined only in multiples of 2π, the coordinate y in equation (10) is, at first, also multivalued. The reason is that in equation (8) the natural logarithm appears, which is known to be an infinitely multivalued function. This multivaluedness may be eliminated by slitting the w-plane along the real axis from $-\infty$ through 0 to w_1 and from $w = 1$ to ∞ (fig. 7); the only thing left to be done is to fix for every logarithm of (8) the branch of function which is to be valid in the Riemann sheet considered: One stipulates that all logarithms on the upper boundary of the slit to the right of $w = \frac{R^2}{w_1}$ assume real positive values and at all other points the values reached by analytical continuation.

Thus the angles $\delta_1, \delta_2, \delta_3$, and δ_4 are also made single-valued: On the upper boundary to the right of $w = \frac{R^2}{w_1}$ they all have the value 0; in the upper semicircle they vary, as shown in figure 8, between 0 and π; in the lower semicircle δ_1 assumes a value between 0 and $-\pi$, δ_2 to δ_4 values between π and 2π.

In order to be able to determine reliably the angles δ_1 to δ_4, it is best to make use of an illustrative experiment: A pointer is connected with the points $w = w_1$, 1, R^2, and $\frac{R^2}{w_1}$ by elastic strings. If the pointer rests on a point of the upper boundary of the slit to the right of $w = \frac{R^2}{w_1}$, all angles between the strings and the positive-real axis are, according to stipulation, equal to zero. If one travels, starting from this position, without passing across the slit, into the upper semiplane, the angles "open" and assume the values given above. The pointer can be brought from the upper to the lower semiplane only through the passage between $w = w_1$ and 1; angles as shown in figure 8(b) are then obtained.

According to figure 4, the hodograph circle and the slit parts of the real axis correspond to the contours of the external-compression inlet: the upper rectilinear inner wall to the right of the stagnation corresponds to the lower boundary of the slit between 0 and w_1, the upper rectilinear inner wall to the left of the stagnation point to the lower boundary of the slit between $-R$ and 0, the upper nose contour to the

lower semicircle, and, lastly, the upper rectilinear outer wall to the lower boundary of the slit between $w = 1$ and R. Correspondingly, one obtains the lower contours of the inlet with external compression from the boundary line of the upper hodograph semicircle and from the upper boundary of the slit; however, one may obtain them in a simpler manner by the mirroring of the upper contours with respect to the symmetry line.

For the boundary lines enumerated above, the general formulas (10) may be simplified quite considerably: Along the upper inner wall $\left(-R \leq w \leq w_i\right)$, since $\delta_1 = -\pi$; $\delta_2 = \delta_3 = \delta_4 = \pi$, $l_1 = w_i - w_1$, $l_2 = 1 - w_1$, $l_3 = R^2 - w_1$, $l_4 = \frac{R^2}{w_i} - w_1$,

$$x = \frac{Q}{2\pi}\left[(1+f)\ln(1-w_1) - \frac{1}{w_i}\ln(w_i - w_1) + \frac{1-f}{R^2}\ln(R^2 - w_1)\right.$$

$$\left. - \frac{w_i}{R^2}\ln\left(\frac{R^2}{w_i} - w_1\right) - \frac{f}{1-w_1} + \frac{f}{R^2 - w_1}\right] + x_o \tag{11}$$

and, bearing equation (5) in mind,

$$y = \frac{Q}{w_i} - h \tag{12}$$

Along the lower inner wall l_1 to l_4 and $\delta_2, \delta_3, \delta_4$ assume the same values as along the upper inner wall; only δ_1 changes its value to π.

Thus the equation remains the same as before for x, whereas one obtains for y, again taking equation (5) into consideration,

$$y = -h \tag{13}$$

If the inlet opening of the external-compression inlet is put equal to $2h$, there follows from equation (12) and equation (13)

$$Q = 2h\, w_i \tag{14}$$

With this value one obtains as final equations for the upper and lower inner wall from equations (11), (12), and (13)

$$\frac{x}{h} = \frac{w_i}{\pi}\left[(1 + f)\ln(1 - w_1) - \frac{1}{w_i}\ln(w_i - w_1) + \frac{1 - f}{R^2}\ln(R^2 - w_1)\right.$$
$$\left. - \frac{w_i}{R^2}\ln\left(\frac{R^2}{w_i} - w_1\right) - \frac{f}{1 - w_1} + \frac{f}{R^2 - w_1}\right] + \frac{x_o}{h} \tag{15}$$

$$\frac{y}{h} = 1, \quad \text{or} \quad \frac{y}{h} = -1, \quad \text{respectively} \tag{15a}$$

Along the upper outer wall $1 \leq w \leq R$ and $\delta_1 = 0$, $\delta_2 = 2\pi$, $\delta_3 = \delta_4 = \pi$, $l_1 = w_1 - w_i$, $l_2 = w_1 - 1$, $l_3 = R^2 - w_1$, $l_4 = \frac{R^2}{w_i} - w_1$, and, taking equations (5) and (14) into consideration, the equations

$$\frac{x}{h} = \frac{w_i}{\pi}\left[(1 + f)\ln(w_1 - 1) - \frac{1}{w_i}\ln(w_1 - w_i) + \frac{1 - f}{R^2}\ln(R^2 - w_1)\right.$$
$$\left. - \frac{w_i}{R^2}\ln\left(\frac{R^2}{w_i} - w_1\right) + \frac{f}{w_1 - 1} + \frac{f}{R^2 - w_1}\right] + \frac{x_o}{h} \tag{16}$$

$$\frac{y}{h} = w_i(1 + f) \tag{16a}$$

are valid. The difference between the constant y-values of the equations (15a) and (16a) is the wall thickness of the external-compression inlet:

$$\frac{d}{h} = w_i(1 + f) - 1 = \frac{(1 - w_i)^2}{R^2 - 1} \tag{17}$$

The hodograph circle itself corresponds to the nose contour. In this case, also, a few simplifications result for the equations (10), due to the fact that $w = w_i$ and $w = \frac{R^2}{w_i}$, $w = 1$ and $w = R^2$ are reflection points of the circle H:

If one applies to l_1, l_4 on one hand and to l_2, l_3 on the other hand the equation (32) of the appendix, putting in the first case $h_1 = l_1$, $h_2 = l_4$, and $w_o = w_i$ and in the second case $h_1 = l_2$, $h_2 = l_3$, and $w_o = 1$, one obtains

$$\frac{l_1}{l_4} = \frac{w_i}{R} \qquad \frac{l_2}{l_3} = \frac{1}{R} \tag{18}$$

If one substitutes, furthermore, in formula (33) of the appendix one time $\gamma_1 = \delta_1$, $\gamma_2 = \delta_4$ and the other time $\gamma_1 = \delta_2$, $\gamma_2 = \delta_3$, one obtains

$$\begin{aligned} \delta_1 + \delta_4 &= \varphi + \pi \\ \delta_2 + \delta_3 &= \varphi + \pi \end{aligned} \tag{19}$$

With equations (18), (19), (14), (5), and (7) one obtains, from equation (10), for the nose contours of the external-compression inlet, the following equations:

$$\begin{aligned} \frac{x}{h} = \frac{w_i}{\pi}\Bigg[& \frac{1}{R^2}\left(\frac{R^2}{w_i} + w_i\right) \ln \frac{l_2}{l_1} + \frac{f}{l_2}\left(\cos \delta_2 + \frac{\cos(\varphi - \delta_2)}{R}\right) \\ & + \frac{f + w_i - 1}{R^2} \ln R + \frac{1}{w_i} \ln w_i + \frac{1 - w_i}{w_i} - \frac{1 - w_i}{R^2}\Bigg] \\ \frac{y}{h} = \frac{w_i}{\pi}\Bigg[& \frac{R^2 - 1 + f(R^2 + 1)}{R^2} \delta_2 + \frac{1}{R^2}\left(w_i - \frac{R^2}{w_i}\right)\delta_1 \\ & - \frac{f}{l_2}\left(\sin \delta_2 + \frac{\sin(\varphi - \delta_2)}{R}\right) + \frac{1 - w_i - f}{R^2}(\varphi + \pi)\Bigg] + 1 \end{aligned} \tag{20}$$

The relation between x and w along the symmetry line, valid for $1 \geq w \geq w_i$ in equations (10) also is useful:

$$\frac{x}{h} = \frac{w_i}{\pi}\left[(1 + f)\ln(1 - w_1) - \frac{1}{w_i}\ln\left(w_1 - w_i\right) + \frac{1 - f}{R^2}\ln\left(R^2 - w_1\right)\right.$$
$$\left. - \frac{w_i}{R^2}\ln\left(\frac{R^2}{w_i} - w_1\right) - \frac{f}{1 - w_1} + \frac{f}{R^2 - w_1}\right] + \frac{x_o}{h} \tag{21}$$

V. ON A MINIMAL CHARACTERISTIC OF THE SIMPLEST SYMMETRICAL INLET WITH EXTERNAL COMPRESSION.

The symmetrical hodograph of section III can easily be somewhat generalized, if one no longer requires coincidence of the center of the hodograph circle with the origin of the w-plane, but admits - within certain arbitrary limits - a position of the center of the circle on the real axis. According to whether the center of the circle lies to the left or right of the origin of the w-plane, the corresponding external-compression inlet assumes nose shapes for which the local velocity downstream increases or decreases.

In order to derive this more general hodograph, one visualizes the circle as lying in a ζ-plane in such a manner that the center of the circle and the origin of the plane coincide (fig. 9). The sink $-Q$ shall lie at ζ_i, the source Q and the doublet M at ζ_∞. According to equations (35) and (36) of the appendix, the complex potential of this flow is

$$F(\zeta) = \frac{Q}{2\pi}\ln\frac{\left(\zeta - \zeta_\infty\right)\left(\zeta - \frac{R^2}{\zeta_\infty}\right)}{\left(\zeta - \zeta_i\right)\left(\zeta - \frac{R^2}{\zeta_i}\right)}$$
$$+ \frac{M}{2\pi}\left\{\frac{1}{\zeta - \zeta_\infty} - \left(\frac{R}{\zeta_\infty}\right)^2\frac{1}{\zeta - \frac{R^2}{\zeta_\infty}}\right\}$$

and with $M = fQ$

$$\frac{dF}{d\zeta} = \frac{Q}{2\pi}\left[\frac{1}{\zeta - \zeta_\infty} - \frac{1}{\zeta - \zeta_1} + \frac{1}{\zeta - \frac{R^2}{\zeta_\infty}} - \frac{1}{\zeta - \frac{R^2}{\zeta_1}}\right.$$

$$\left. - f\left\{\left[\frac{1}{(\zeta - \zeta_\infty)^2} - \left(\frac{R}{\zeta_\infty}\right)^2 \frac{1}{\left(\zeta - \frac{R^2}{\zeta_\infty}\right)^2}\right]\right\}\right] \tag{22}$$

The point $\zeta = \zeta_o$ is assumed to be a stagnation point; then, according to equation (22), necessarily

$$\frac{1}{\zeta_o - \zeta_\infty} - \frac{1}{\zeta_o - \zeta_1} + \frac{1}{\zeta_o - \frac{R^2}{\zeta_\infty}} - \frac{1}{\zeta_o - \frac{R^2}{\zeta_1}}$$

$$= f\left\{\left[\frac{1}{(\zeta - \zeta_\infty)^2} - \left(\frac{R}{\zeta_\infty}\right)^2 \frac{1}{\left(\zeta - \frac{R^2}{\zeta_\infty}\right)^2}\right]\right\} \tag{23}$$

Since, according to the expositions of section II the stagnation point ζ_o must coincide with the zero point of the w-plane, ζ_1 with w_1, and ζ_∞ with $w_\infty = 1$, there exist the relations

$$w = \zeta - \zeta_o$$

$$w_1 = \zeta_1 - \zeta_o \tag{24}$$

$$1 = \zeta_\infty - \zeta_o$$

and from equation (23) follows

$$f = \frac{\frac{1}{w_i} - 1 + \frac{1 + \zeta_o}{\zeta_o^2 + \zeta_o - R^2} - \frac{w_i + \zeta_o}{\zeta_o^2 + w_i\zeta_o - R^2}}{1 - \frac{R^2}{\left(\zeta_o^2 + \zeta_o - R^2\right)^2}} \tag{25}$$

According to equation (2),

$$z = \int \frac{dF}{dw}\frac{dw}{w} + \text{const} = \int \frac{dF}{d\zeta}\frac{d\zeta}{w(\zeta)} + \text{const}$$

and one obtains with equations (22) and (24), taking equation (25) into consideration, after some calculating

$$z = \frac{Q}{2\pi}\left[\frac{f}{\zeta - \zeta_\infty} - \frac{f\left(\frac{R}{\zeta_\infty}\right)^2}{\frac{R^2}{\zeta_\infty} - \zeta_o}\,\frac{1}{\zeta - \frac{R^2}{\zeta_\infty}} + (1 + f)\ln\left(\zeta - \zeta_\infty\right)\right.$$

$$+ \left(1 - \frac{f\left(\frac{R}{\zeta_\infty}\right)^2}{\frac{R^2}{\zeta_\infty} - \zeta_o}\right)\frac{\ln\left(\zeta - \frac{R^2}{\zeta_\infty}\right)}{\frac{R^2}{\zeta_\infty} - \zeta_o} - \frac{1}{w_i}\ln\left(\zeta - \zeta_i\right) \tag{26}$$

$$\left. - \frac{\ln\left(\zeta - \frac{R^2}{\zeta_i}\right)}{\frac{R^2}{\zeta_i} - \zeta_o}\right] + \text{const}$$

In order to make here again the logarithms single-valued, the ζ-plane must be slit from $-\infty$ to $\zeta_i = w_i + \zeta_o$ and from $\zeta_\infty = 1 + \zeta_o$ to ∞.

The two slit boundaries represent the rectilinear wall parts of the external-compression inlet, in particular, the upper boundary of the left slit, the lower inner wall, the upper boundary of the right slit, the lower outer wall. The distance between the walls equals the difference of the corresponding imaginary parts of equation (26)

$$d = \frac{Q}{2}\left[-\frac{1}{w_i} + (1 + f)\right]$$

The inlet opening of the external-compression inlet results as the difference between the imaginary parts of equation (26) for the two boundaries of the left slit

$$2h = \frac{Q}{w_i}$$

and with this relation one finally obtains the old formula (17) for the wall thickness of the external-compression inlet.

$$\frac{d}{h} = w_i(1 + f) - 1$$

The maximum velocity is, according to equation (24) and fig. 9,

$$w_{max} = R + \zeta_o \quad \text{for} \quad \zeta_o \geq 0$$

$$w_{max} = R - \zeta_o \quad \text{for} \quad \zeta_o \leq 0 \qquad (27)$$

ζ_o must not be selected quite arbitrarily but always so that ζ_o, ζ_i, and ζ_∞ lie still inside of the circle H. Hence follows according to figure 10 the admissible domain for ζ_o:

$$-R \leq \zeta_o \leq R - 1$$

If not R but the maximum velocities are fixed, the domain of ζ_o may be expressed, by means of equation (27), by

$$-\frac{w_{max}}{2} \leq \zeta_o \leq \frac{w_{max} - 1}{2}$$

If ζ_o is varied within this domain while w_{max} is held constant, the wall thickness of the external-compression inlet changes. As figure 11 shows for the examples $\frac{w_{max}}{w_\infty} = 1.2$, $\frac{w_i}{w_\infty} = 0.1, 0.4, 0.7$, the wall thickness has at $\zeta_o = 0$ a definite minimum. The proof that this must always be so requires a very complicated argument, since the minimum lies precisely at the section point of the curves more closely determined by the equations (27). However, the proof may be omitted, particularly since one may readily conclude from the relatively simple calculation of further examples that the above statement is generally valid.

In the case $\zeta_o = 0$ the center of the hodograph circle coincides with the origin of the w-plane, and one obtains the important statement: Of all symmetrical external-compression inlets considered here, the one treated first, namely, the external-compression inlet with constant velocity along its entire nose contour, has for equal excess velocity and equal pressure conversion the smallest wall thickness.

VI. VELOCITY AND PRESSURE DISTRIBUTIONS, THRUST.

In determining the contours and stream lines of the external-compression inlet one obtains the corresponding velocity and pressure distributions almost without further calculation:

The complex velocity w is the coordinate of the hodograph. The square of its magnitude is, according to equation (9),

$$|w|^2 = w_1^2 + w_2^2$$

If one puts the pressure of the undisturbed velocity equal to zero,

$$\frac{p}{q} = 1 - \frac{|w|^2}{w_\infty^2}$$

and because $w_\infty = 1$

$$\frac{p}{\frac{\rho}{2} w_\infty^2} = 1 - \left(w_1^2 + w_2^2\right) \tag{28}$$

Along the entire nose contour of the simplest external-compression inlet of section IV,

$$|w|^2 = \text{const} = R^2$$

and

$$p_{nose} = \frac{\rho}{2} w_\infty^2 \left(1 - R^2\right)$$

is the constant negative pressure which acts perpendicularly on a surface element of the nose (fig. 12). The force component opposite the free-stream direction is

$$dS = p_{nose} \frac{dy}{ds} ds$$

and the thrust exerted on a nose contour

$$\frac{S}{2} = \int_h^{h+d} p_{nose}\, dy = \frac{\rho}{2} w_\infty^2 \left(1 - R^2\right) d$$

The nose thrust of the entire external-compression inlet is with equation (17)*

$$S = -\rho w_\infty^2 h \left(1 - \frac{w_i}{w_\infty}\right)^2 \tag{29}$$

*For a clearer presentation of formula (29) it is expedient to designate the velocity ratio (velocity in the interior of the device to free-stream velocity) no longer by $w_i/1$, but by w_i/w_∞.

This simple equation for the nose thrust is derived, at first, only for the "simplest" symmetrical external-compression inlets of section IV; however, the very notable fact alone, that apart from the open height 2h no further form parameter enters into the equation, permits the conclusion that it must have a more general significance.

For better understanding one visualizes a control area lying about an arbitrary two-dimensional external-compression inlet (fig. 13); the inlet must satisfy one condition only: that its walls in the downstream direction tend toward infinity with constant thickness. The points 1, 2, 3, 4 are to be so far removed from the entrance of the inlet that the horizontal component of the velocity practically equals w_∞ or w_i, respectively.* But even in this case the horizontal control areas 1, 2, and 3, 4 cannot be flow surfaces but, for reasons of continuity, the quantity of fluid

$$Q_{1,2} + Q_{3,4} = (2h + d_o + d_u) w_\infty - 2h\, w_i \tag{30}$$

must flow through them. For the total nose thrust the momentum equation gives the value

$$S = S_o + S_u = \rho w_\infty^2 (2h + d_o + d_u) - (p_i + \rho w_i^2) 2h - (Q_{1,2} + Q_{3,4}) \rho w_\infty \tag{31}$$

With equation (30) and

$$p_i = \frac{\rho}{2} w_\infty^2 - \frac{\rho}{2} w_i^2$$

one obtains from equation (31) after a short calculation again the equation (29); the latter's validity for arbitrary external-compression inlet forms is therewith proved. For the rest, one can easily find out

*The disturbance velocities which were neglected here and further on become - as can be easily proved - with increasing distance from the entrance of the external-compression inlet "small of the first order." Since the control area also increases linearly with the distance of the points 1, 2, 3, 4 from the entrance of the external-compression inlet, all integrals of quadratic products of the disturbance velocities must disappear in the limiting process, whereas the integrals of linear terms of the disturbance velocities remain finite. With these facts taken into consideration, it is easy to give exact proof for equations (30) and (31).

that, under analogous presuppositions, this equation is valid also for the nose thrust of the internal-compression inlets.

VII. NUMERICAL EXAMPLES AND DERIVED INLETS.

Before the theory of the two-dimensional external-compression inlet developed above is illustrated by a few numerical examples, the aims and range of this theory shall once more be briefly represented: Under the assumption of incompressible frictionless fluid the contours and the pressure distribution of the external-compression inlet are calculable for a prescribed velocity ratio w_i/w_∞ and a prescribed maximum velocity w_{max}/w_∞.

The maximum velocity is assumed on the curved nose contour. In the pressure distribution along the nose contour one can distinguish three different types of external-compression inlets which may be comprised by the theory: types where the velocity downstream along the nose contour has a continuous increase, or a continuous decrease, or remains constant. The property named last is the special characteristic of the so-called "simplest symmetrical external-compression inlet."

Apart from the shape of the nose contour, the maximum wall thickness of the external-compression inlet also is decisive for the magnitude of the maximum velocity, inasmuch as the maximum excess velocity may be kept smaller with increasing wall thickness. The simplest symmetrical external-compression inlet is distinguished among all other inlets of the kind considered here by possessing, for a wall thickness kept constant, the smallest excess velocity or, inversely, for an excess velocity kept constant, the smallest wall thickness. This property makes the simplest symmetrical external-compression inlet particularly suitable for practical applications; hence the following numerical examples are limited to that inlet.

The following should be noted about the general form of the symmetrical inlet with external compression: Inner and outer wall are rectilinear and both run parallel to the free-stream direction. The only curved contour is the nose contour which connects the outer and inner wall without a break but with a sudden change in curvature at the transition points.

It is a minor inconvenience that one obtains, on principle, for two different pairs of values w_i/w_∞, w_{max}/w_∞ forms of external-compression inlets which also are different and that, according to the theory existing so far, it is not possible, for instance, to retain the form calculated for a pair of values w_i/w_∞, w_{max}/w_∞ and to determine pressure and velocity distribution for another w_i/w_∞. This disadvantage could be

eliminated by a suitable mapping of the hodograph circle onto another simply connected surface; however, simplicity and clearness of the theory would suffer so greatly that it seemed better to omit this step for the time being. Effects and partial circumvention of the limitation just mentioned will be discussed later.

We now turn to individual discussion of numerical results. In figure 14 the wall thickness (d) referred to the inlet half-height (h) is represented as function of w_{max}/w_∞. The corresponding equation is equation (17) in which one has to substitute $R = w_{max}$. One recognizes that d/h retains a finite value even for $w_i/w_\infty = 0$, if $w_{max} > w_\infty$ is admitted but that, however, on the other hand, d/h assumes infinite magnitude for any w_i/w_∞, if $w_{max} = w_\infty$ is required. As mentioned before, the wall thickness shows a continuous increase with decreasing maximum velocity. Down to $w_{max} = 2.5\ w_\infty$ this increase is practically insignificant. In order to give a clearer picture of the interesting domain $w_{max} < 2.5\ w_\infty$, it has been represented once more to an enlarged velocity scale in figure 14. It is shown that the inlet with purely external compression requires, for small w_i, quite considerable wall thicknesses, if the value w_{max}/w_∞ must not become very much larger than 1. For $w_i/w_\infty = 0$, for instance, the excess velocity can, for $d/h = 1$, be lowered not further than $w_{max}/w_\infty = 1.42$. However, $d/h = 1$ signifies that the total wall thickness equals the total height of inlet opening. $w_i/w_\infty = 0$ is an operating condition which in no way answers the purpose of the inlet and has, therefore, no decisive significance for its design. That operating condition is of interest only as a boundary case for the estimation of most unfavorable conditions. However, figure 14 shows that, due to the steep ascent of the curves in the left part of the diagram, the wall-thickness ratio does not become much more favorable even for, for instance, $w_i/w_\infty = 0.1$.

Figures 15 to 18 represent a few calculated examples of symmetrical inlets with external compression, corresponding to the parameters $w_i/w_\infty = 0.1$ and 0.4, $w_{max}/w_\infty = 1.4$; $w_i/w_\infty = 0.1$ and 0.4, $w_{max}/w_\infty = 1.2$. The fixed walls are cross-hatched. At the same time the stagnation-point stream lines are drawn in to give an excellent impression of the velocity retardation ahead of the inlet entrance. The figures confirm the fact discussed before: that the wall thickness of the external-compression inlet is bound to increase for decreasing w_{max}/w_∞ as well as for decreasing w_i/w_∞. A comparison of figures 15 and 16 on one hand with figures 17, and 18 on the other shows, moreover, that the curvature of the nose contour

must be the flatter and, consequently, its length the greater, the smaller the excess velocity is to be kept. The relatively "sharp-pointed nose," especially, is surprising, particularly for the external-compression inlets for $w_i/w_\infty = 0.1$ with their stagnation points situated relatively far to the rear.

In order to estimate the behavior of the external-compression inlets for other conditions of retardation, one could follow the procedure shown in the example of figure 15. That external-compression inlet has the wall thickness $d/h = 0.845$. If the wall thickness alone were responsible for the magnitude of the excess velocity w_{max}/w_∞, the w_{max}/w_∞ for other velocity ratios w_i/w_∞ could be easily determined from figure 14 by having there a parallel to the abscissa go through $d/h = 0.845$. For $w_i/w_\infty = 0.4$ one would thus obtain $w_{max}/w_\infty = 1.195$. However, figure 17 shows for $w_i/w_\infty = 0.4$ and $w_{max}/w_\infty = 1.2$ that the nose, for such a low excess velocity, must have a considerably flatter curvature; one may draw the conclusion that, for $w_i/w_\infty = 0.4$, w_{max}/w_∞ actually will slightly exceed the value determined above from figure 14. The reason lies, above all, in the fact that the velocity along the nose contour of the external-compression inlet of figure 15 is no longer constant for $w_i/w_\infty = 0.4$. Anyway, this deliberation shows that the excess velocity will probably never exceed $w_{max}/w_\infty = 1.4$, if the external-compression inlet of figure 15 for $w_i/w_\infty = 0.4$ is being used. Further clarification of this state of affairs is up to wind tunnel tests for the time being.

Apart from the external-compression inlet contours, the symmetry stream lines, and the stagnation point stream lines, the most important pressure distributions also are plotted in figures 15 to 18: above the external-compression inlet the pressure distribution along the symmetry stream line, below it the pressure distribution along the wall contour. The first pressure distribution shows that the pressure conversion takes place to the greatest part before the entrance into the external-compression inlet and that it is, at any rate, practically completed at $x/h = 1$. This statement about the rearward shift of the "completed pressure conversion" also follows from the pressure distribution along the inner wall. It is of importance if one wants to change the inlet with purely external compression to an intermediate form, as defined in section I, by reducing the wall thickness from the inside (fig. 19). Consequently, the enlargement of the inner cross section probably must not occur before $x/h = 1$. Of course, it must be even then introduced with a very flat curvature in order to avoid disturbances of the pressure conversion at the entrance that could be caused by the influence of the negative pressures U (fig. 19). The clarification of this problem also must be left to the wind tunnel test.

The pressure distribution along the outer wall shows very clearly the constancy of the velocity along the nose contour. The short line

protruding at the left is actually to be regarded as a double line, the upper boundary of which represents a part of the pressure distribution of the inner nose contour. The cause of the large pressure drop at the end of the outer nose contour is the aforementioned sudden change in curvature at the transition from the nose contour to the rectilinear outer wall. Comparatively slowly, the pressure along this wall is gradually reduced to the undisturbed pressure, the more slowly, the smaller the excess velocity w_{max}/w_∞ has been kept.

If one makes the symmetry stream line the solid wall, one obtains external-compression inlets as they could be applied, for instance, for underslung radiators or divergent-nozzle radiators, which are located on the pressure side of a wing (fig. 20). If such an inlet is not constructed as a retractable device, it must be designed according to the same points of view as the symmetrical external-compression inlet, that is, wall thickness and nose contour are to be proportioned for the minimum w_i/w_∞ and the maximum admissible w_{max}/w_∞. For larger w_i/w_∞, w_{max}/w_∞ then stays automatically below the admissible limit.

It can be seen that the wall thickness may be kept thinner when the device is retractable. For proof, one starts from half the external-compression inlet for $w_i/w_\infty = 0.4$, $w_{max}/w_\infty = 1.2$. The inlet height is assumed to be $h_{0.4}$, the wall thickness $d_{0.4}$. According to figure 14, $(d/h)_{0.4}$ equals 0.82. For the same excess velocity, but with $w_i/w_\infty = 0.1$, $(d/h)_{0.1} = 1.83$. In figure 21(a) the contours of the two external-compression inlets are drawn on top of each other in such a manner that the scale of the first inlet is the same as in figure 18; the scale of the second, however, is no longer the same as in figure 17, but was reduced by the factor $0.82/1.83 = 0.45$. The contours almost coincide and permit the conclusion that the excess velocity w_{max}/w_∞ is not considerably exceeded if the inlet height of the external-compression inlet of figure 18 is reduced from $h_{0.4}$ to $0.45\ h_{0.4}$ while simultaneously the retardation is reduced to $w_i/w_\infty = 0.1$ (fig. 21(b)). However, the air quantity taken out of the free stream is thereby reduced by the factor $(0.45)(0.1/0.4) = 0.11$. Similar conditions exist if one starts from the external-compression inlet for $w_i/w_\infty = 0.4$, $w_{max}/w_\infty = 1.4$ (fig. 22).

Instead of the symmetry streamline, any other streamline can be made the solid wall and thus obtain forms corresponding to divergent-nozzle radiators where the radiator block is partly retracted into the pressure side of the wing (figs. 23 and 25). The maximum of this one-sided displacement is indicated by the stagnation-point streamline and inner wall. In figure 23 it is represented for the external-compression

inlet $w_i/w_\infty = 0.1$, $w_{max}/w_\infty = 1.4$. Difficulties will probably arise due to the fact that even the thin pressure-side boundary layer is not able to overcome the pressure increase at the stagnation point S.

Conditions are more favorable if a streamline is selected as solid wall along which the pressure increases continuously and monotonically up to its final pressure.* This is certainly the case for instance for the symmetry streamline. However, there are other streamlines as well which satisfy this condition. In the hodograph they appear as streamlines which lie outside of a circle about the zero point, the radius of which is w_i/w_∞. In the hodograph of figure 24 a streamline is represented which barely satisfies this requirement ($\psi = 3\pi/10$). For this streamline the corresponding one of the external-compression inlet was calculated and made the solid wall (figure 25). One recognizes that it is permissible to retract the radiator block to a much smaller degree than is customary in present designs. For the rest it should be noted that the possibility of a flow separation at the upper wall must be considered also for the design according to figure 25 for $w_i/w_\infty \gg 0.1$; all streamlines, therefore, show, for larger w_i/w_∞, a considerably flatter course, and one can easily overstep again the barely admissible one-sided displacement which is characterized by the stagnation-point streamline.

VIII. APPENDIX.

a. Auxiliary Theorems Concerning Points Reflected on the Circle.

Without limitation of generality one may assume that the two reflection points lie on the real axis. If $w = w_o$ is a real point in the interior of the circle, then R^2/w_o is its reflection point with respect to the circle H of radius R which was drawn about the origin of the w-plane. If, furthermore, h_1 and h_2 are the rays from these points to the point $w = Re^{i\varphi}$ (see fig. 26) and γ_1, γ_2 the angles formed by these rays with the real axis, then according to the cosine law,

*In this case it is at least ensured that the pressure will nowhere be larger, the velocity nowhere smaller than the end pressure and end velocity, respectively.

$$h_1^2 = R^2 - 2Rw_o \cos \varphi + w_o^2$$

$$h_2^2 = \left(\frac{R}{w_o}\right)^2 \left(R^2 - 2Rw_o \cos \varphi + w_o^2\right)$$

and

$$\frac{h_1}{h_2} = \frac{w_o}{R} \tag{32}$$

That means, the ratio of the two rays from two reflection points to a point of the periphery of the circle is independent of φ and thus constant on the entire circle.

Any circle drawn through the two reflection points is known to intersect perpendicularly the circle H. This applies also to the circle K in figure 26. According to a well-known theorem concerning the angle between chord and tangent $\gamma_3 = \pi - \gamma_2$ and according to the external-angle theorem $\gamma_1 = \varphi + \gamma_3$. Hence follows

$$\gamma_1 + \gamma_2 = \varphi + \pi \tag{33}$$

b. Reflection of Source and Doublet on the Circle.

$R > 1$ is again assumed as radius of the circle H, the center of which coincides with the origin of the coordinates. w_o is assumed to be a point of the real axis in the interior of the circle. At that point the complex potential function is to possess the same singularity which would pertain to a single source, namely the singularity $\frac{Q}{2\pi} \ln\left(w - w_o\right)$. If the circle is to become streamline, first, for reasons of continuity, a sink of the same strength as the source must be placed in the interior of the circle, for instance at the zero point. If this source-sink pair is reflected on the circle, an additional source at the point $w = \frac{R^2}{w_o}$ and a sink at $w = \infty$ are added. The complex total potential of the entire system (fig. 27) reads

$$F_Q = \frac{Q}{2\pi} \left[\ln\left(w - w_o\right) + \ln\left(w - \frac{R^2}{w_o}\right) - \ln w\right] \tag{34a}$$

It is easily proved that this potential contains the circle as streamline: With the symbols of appendix a the equation (33) may be written for an arbitrary point of the circle contour in the following form:

$$F_Q = \frac{Q}{2\pi}\left[\ln h_1 + \ln h_2 - \ln R + i\{\gamma_1 + \gamma_2 - \varphi\}\right]$$

The imaginary part of F_Q is, according to equation (33), constant along the entire contour of the circle. Therewith the assertion is already proved.

Concerning the complex potential function (34a) it is, at first, slightly disturbing that, aside from the desired singularity at the point $w = w_o$, another one at the point $w = 0$ must be accepted. However, if one has within the circle at a real point w_o^* a sink of the same strength, the function

$$F_S = -\frac{Q}{2\pi}\left[\ln\left(w - w_o^*\right) + \ln\left(w - \frac{R^2}{w_o^*}\right) - \ln w\right] \qquad (34b)$$

is to be added to equation (34(a)), and the auxiliary sink at $w = 0$ is cancelled against an auxiliary source of the same strength.

For the flow of the hodograph considered above the source is situated at $w = 1$ or ζ_∞, the sink at $w = w_i$ or ζ_i, and the corresponding complex partial potential reads

$$F = \frac{Q}{2\pi}\ln\frac{(w-1)(w-R^2)}{\left(w - w_i\right)\left(w - \frac{R^2}{w_i}\right)} \quad \text{or} \quad \frac{Q}{2\pi}\ln\frac{\left(\zeta - \zeta_\infty\right)\left(\zeta - \frac{R^2}{\zeta_\infty}\right)}{\left(\zeta - \zeta_i\right)\left(\zeta - \frac{R^2}{\zeta_i}\right)} \qquad (35)$$

As is well known, one may obtain the complex doublet potential by placing a sink $-Q$ beside the source Q at the distance h and then permitting the sink to move into the source, while Q simultaneously must become indefinitely large so that Qh converges toward a finite value M. If this method is applied to the system of figure 27, first the scheme of singularities of figure 28 is obtained, the complex potential of which is

$$F = \frac{Q}{2\pi}\left[\left\{\ln\left(w - w_o\right) - \ln\left(w - \left(w_o + h\right)\right)\right\} + \left\{\ln\left(w - \frac{R^2}{w_o}\right) - \ln\left(w - \frac{R^2}{w_o + h}\right)\right\}\right]$$

If one develops the braces in powers of h and then approaches the limit $h = 0$,

$$F_\vartheta = \frac{M}{2\pi}\left[\frac{1}{w - w_o} - \left(\frac{R}{w_o}\right)^2 \frac{1}{w - \frac{R^2}{w_o}}\right]$$

is the complex potential of a doublet in the circle. For the hodographs considered above, the doublet is located at the point $w_o = 1$ or ζ_∞, respectively. The doublet potential then reads

$$F_\vartheta = \frac{M}{2\pi}\left[\frac{1}{w - 1} - \frac{R^2}{w - R^2}\right] \tag{36}$$

or

$$= \frac{M}{2\pi}\left[\frac{1}{\zeta - \zeta_\infty} - \left(\frac{R}{\zeta_\infty}\right)^2 \frac{1}{\zeta - \frac{R^2}{\zeta_\infty}}\right]$$

Translated by Mary L. Mahler
National Advisory Committee
for Aeronautics.

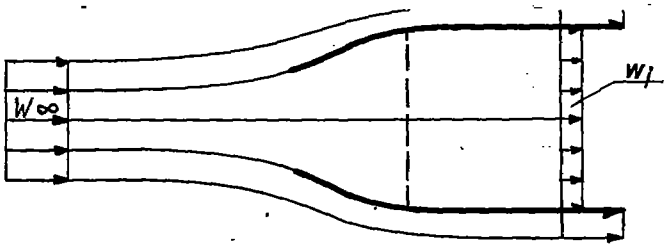

Figure 1.- Internal-compression inlet.

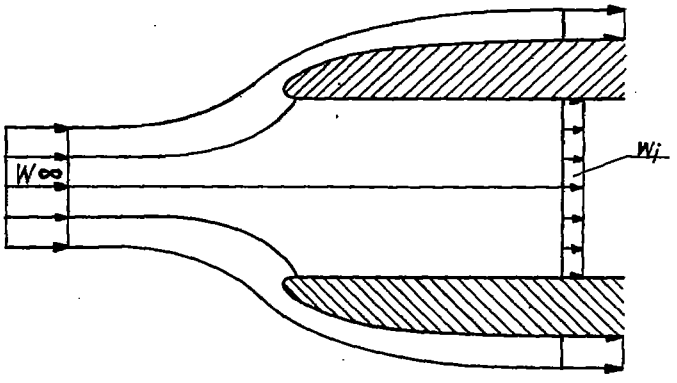

Figure 2.- External-compression inlet.

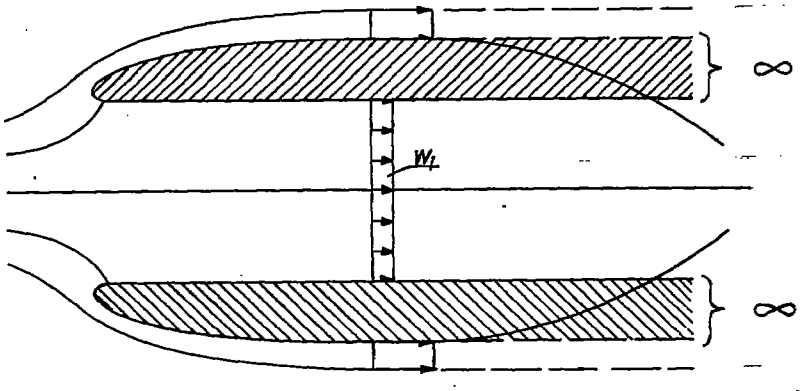

Figure 3.- The theory considers instead of the external-compression inlet of finite length an external-compression inlet, the walls of which extend downstream to infinity.

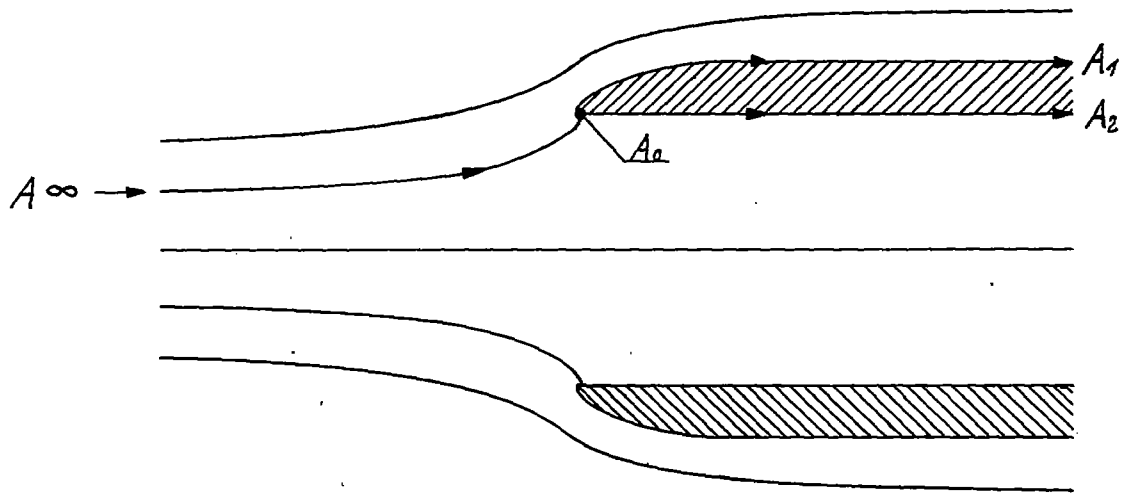

Figure 4(a).- Qualitative stream-line pattern of the external-compression inlet.

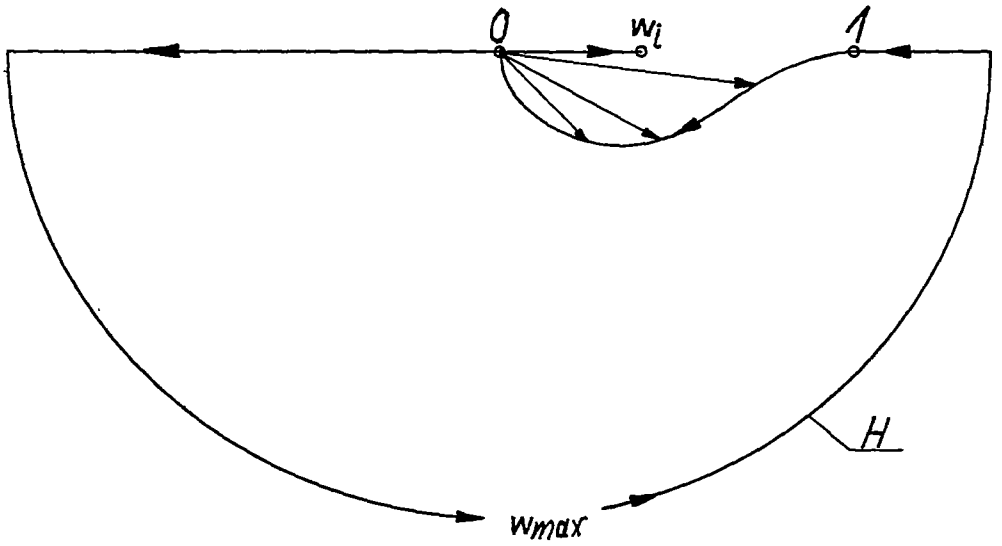

Figure 4(b).- In the hodograph mapping the line 1, 0, w_{max}, 1 corresponds to the stream line A_∞, A_0, A_1, the line 1, 0, w_i to the stream line A_∞, A_0, A_2.

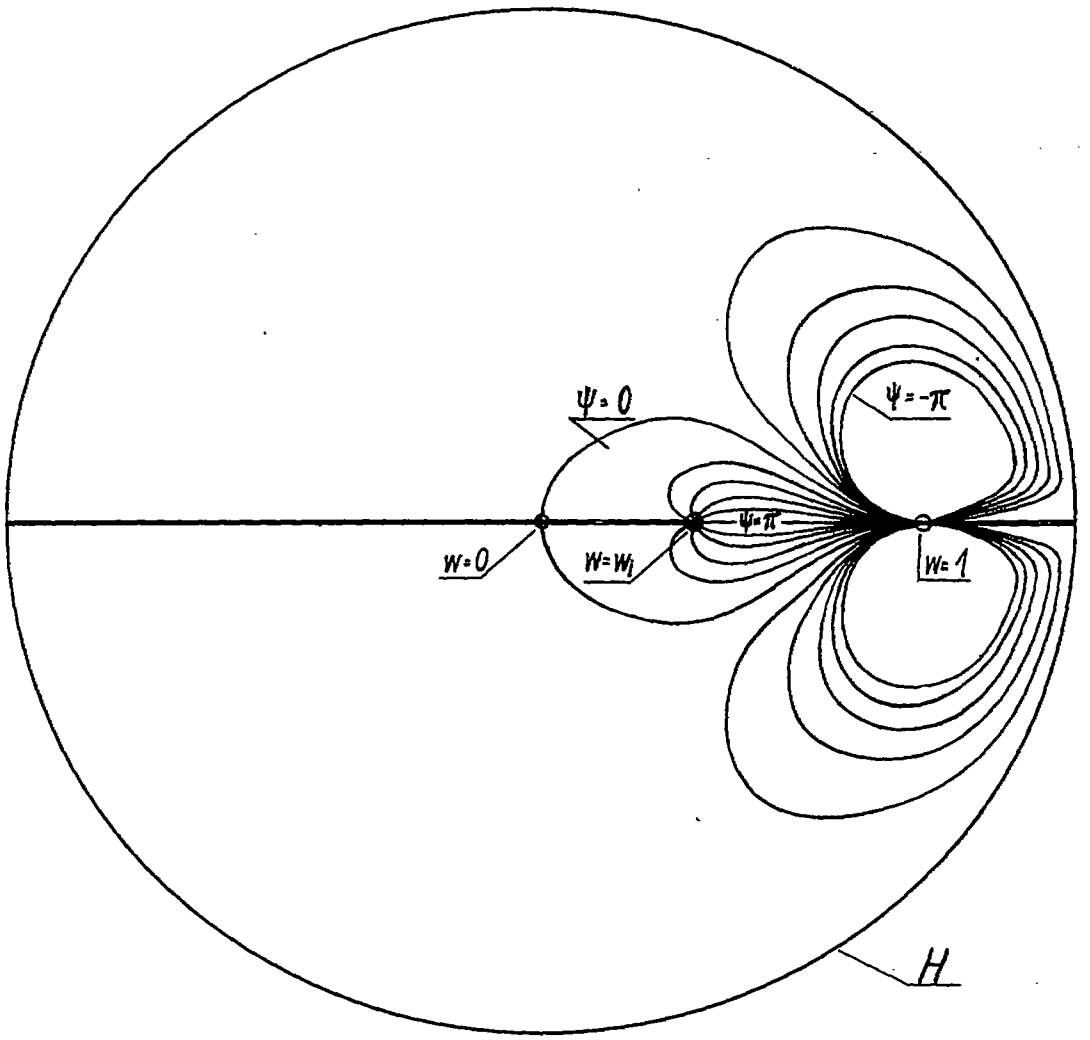

Figure 5.- Hodograph of the simplest symmetrical inlet with external compression for $w_i/w_\infty = 0.4$, $w_{max}/w_\infty = 1.4$.

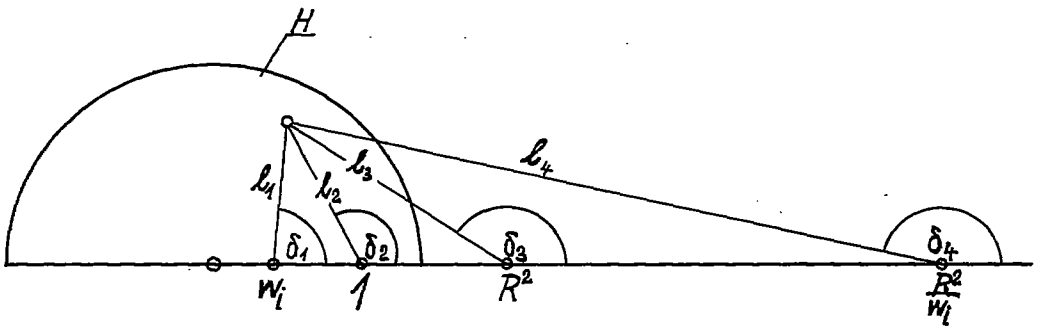

Figure 6.- Definition of the rays l_ν and the angles δ_ν in the w-plane.

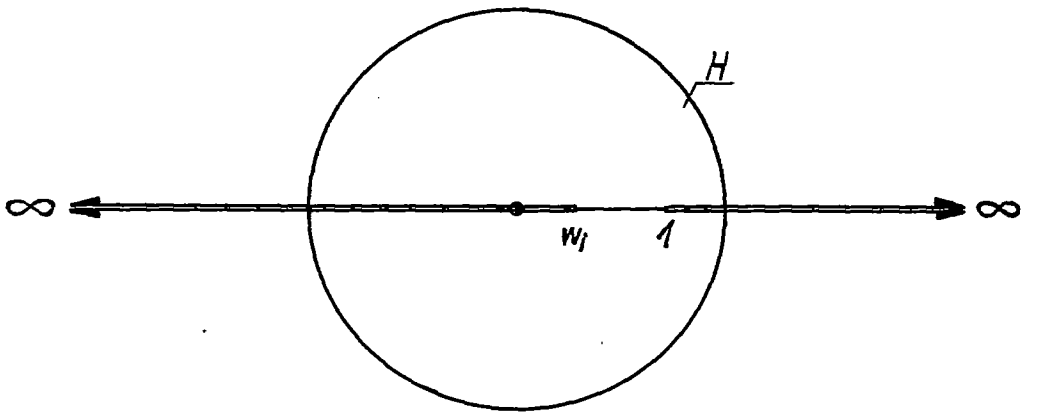

Figure 7.- Slits of the w-plane.

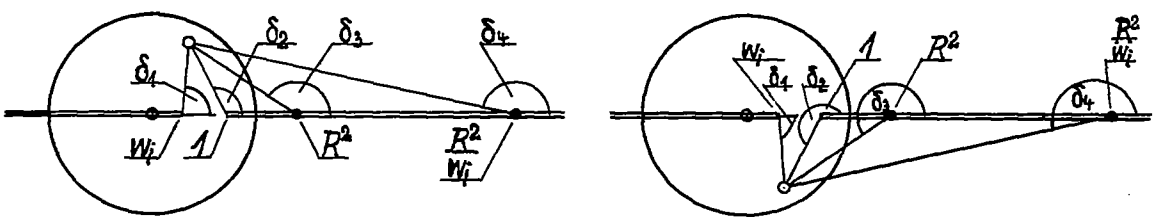

Figure 8.- Definition of the domain of angles in the upper (a) and lower (b) w-semiplane.

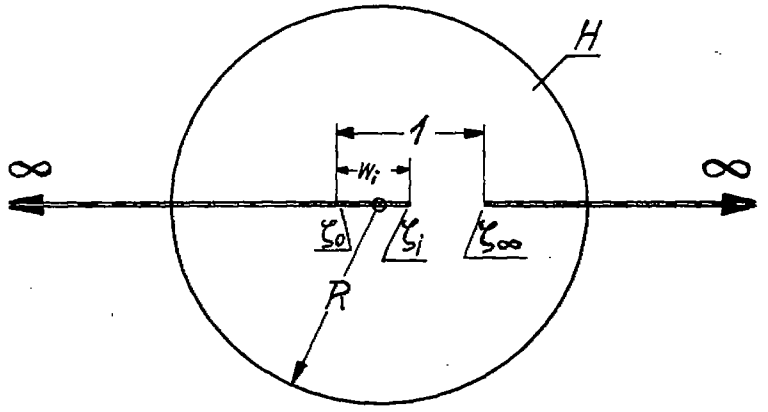

Figure 9.- The generalized symmetrical hodograph in the slit ζ - plane.

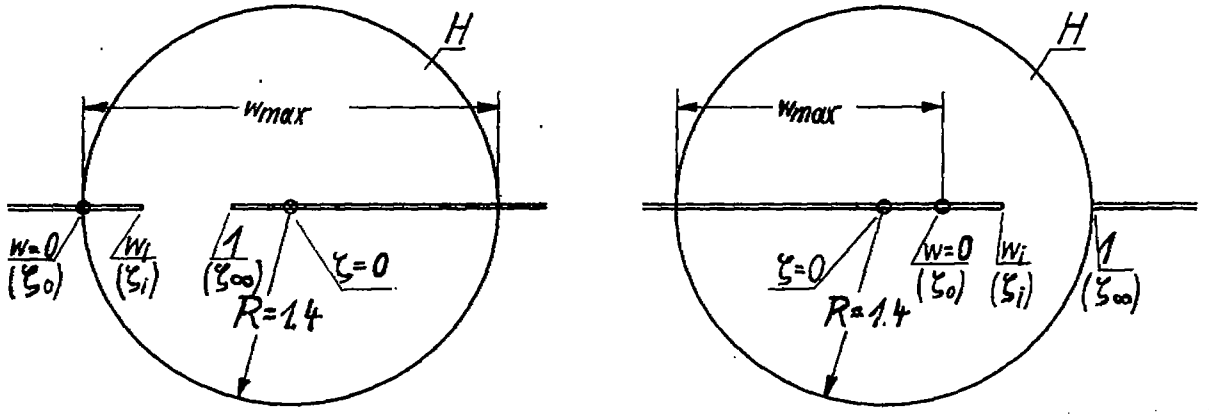

Figure 10.- Extreme positions of the generalized hodograph in the w-plane for fixed w_i and R.

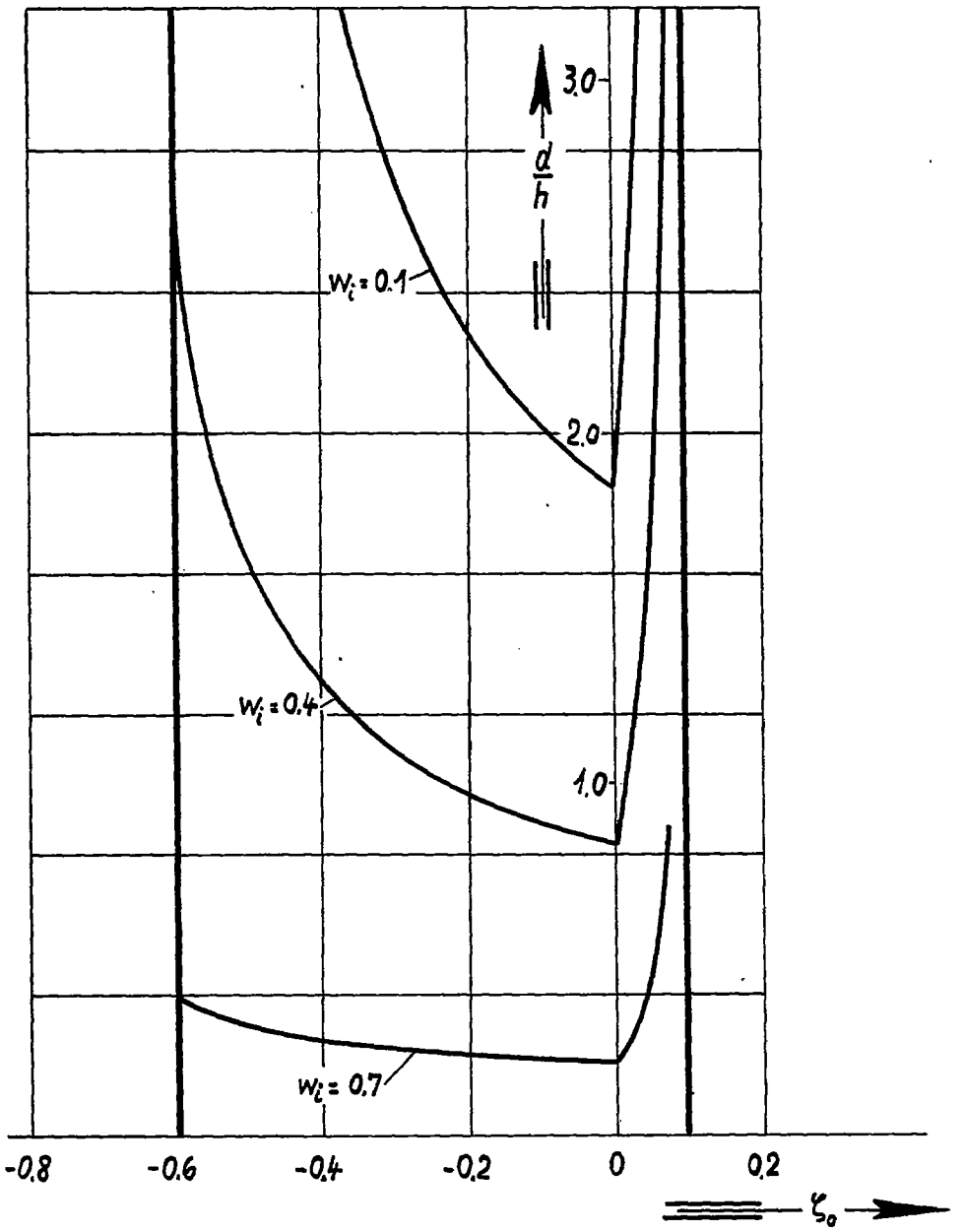

Figure 11.- The ratio of the wall thickness to the half opening height for the generalized symmetrical inlet with external compression as a function of ζ_o for a constant $w_{max}/w_\infty = 1.2$ for $w_i/w_\infty = 0.1, 0.4, 0.7$. For the hodograph of the simplest symmetrical inlet with external compression of sections III and IV, ζ_o equals zero, and d/h is a minimum.

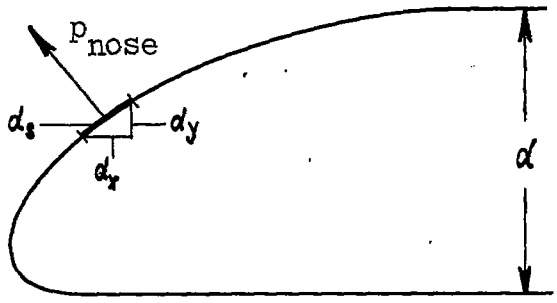

Figure 12.- Concerning the determination of the nose thrust by integration of the pressure distribution.

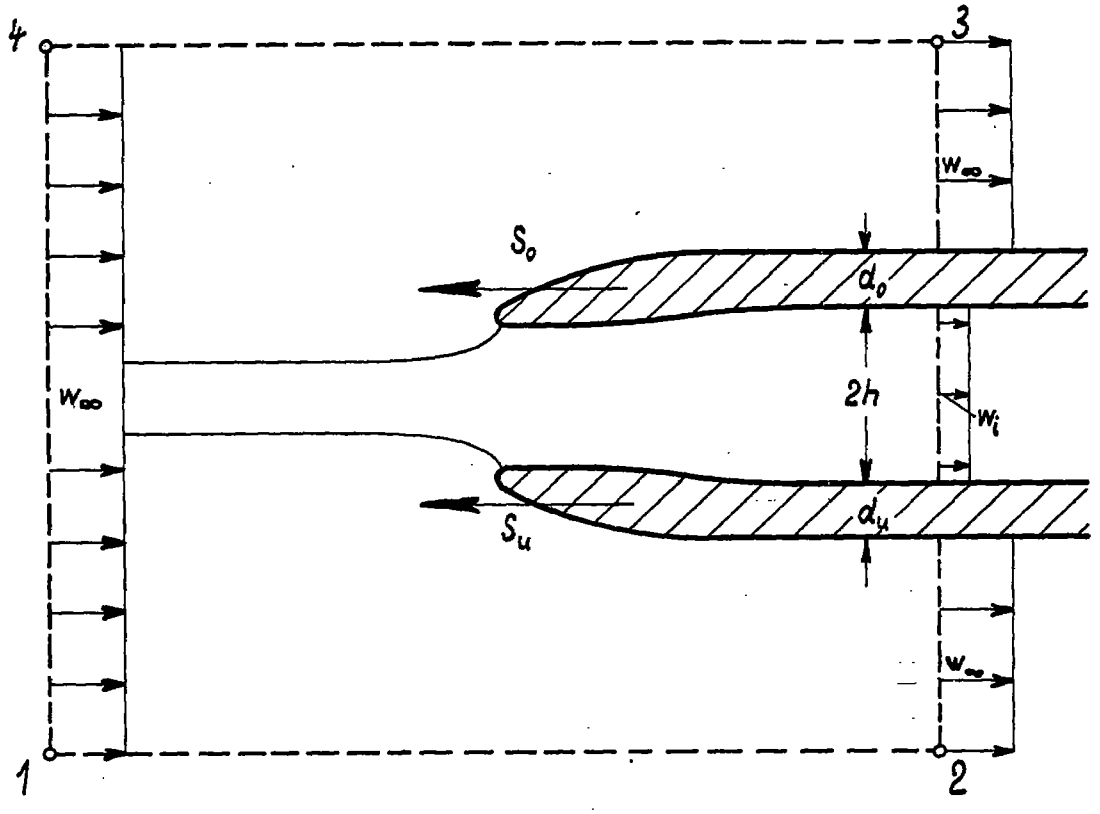

Figure 13.- Concerning the determination of the nose thrust by means of the momentum theorem.

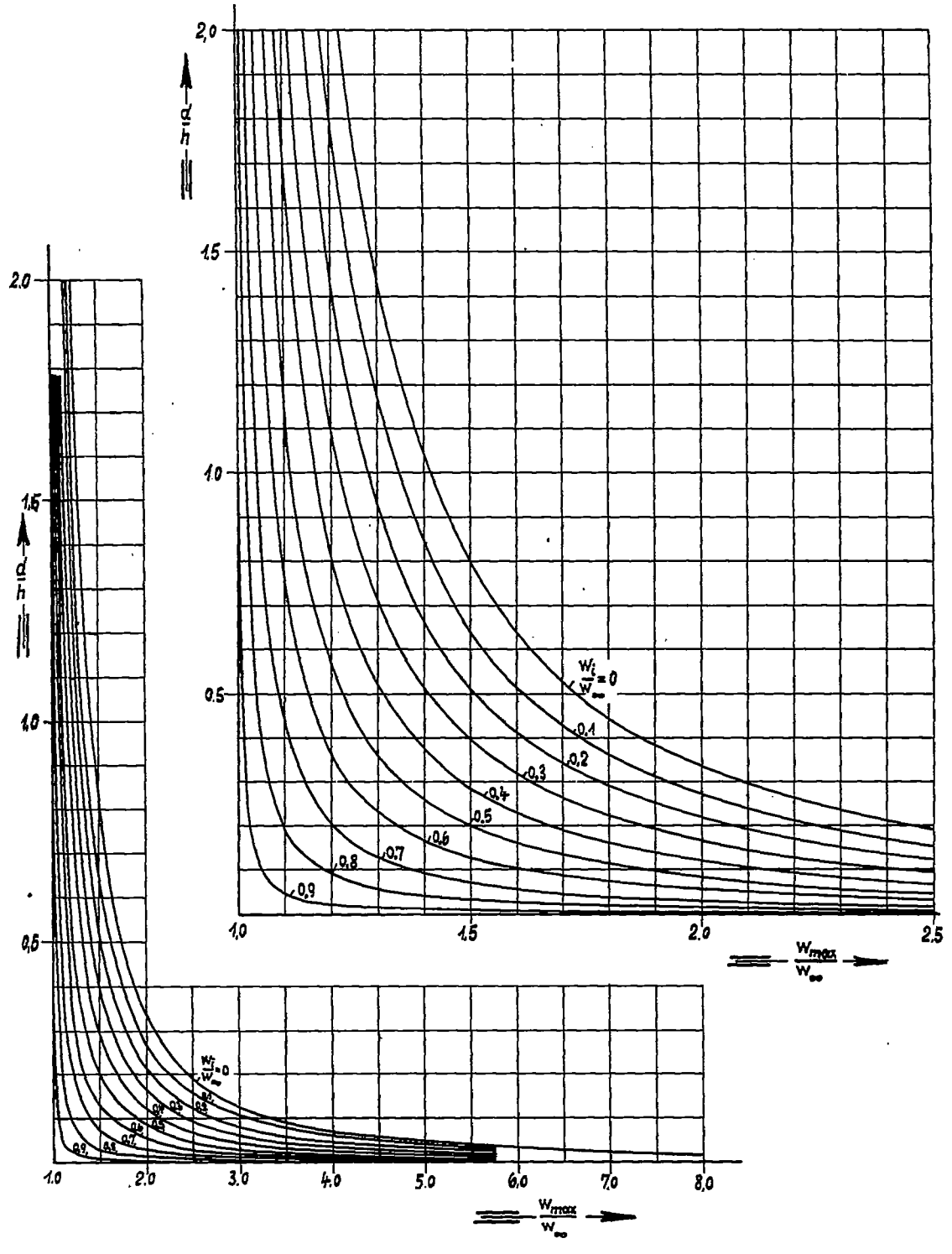

Figure 14.- The ratio d/h for the simplest symmetrical inlet with external compression as a function of w_{max}/w_∞ and w_i/w_∞ .

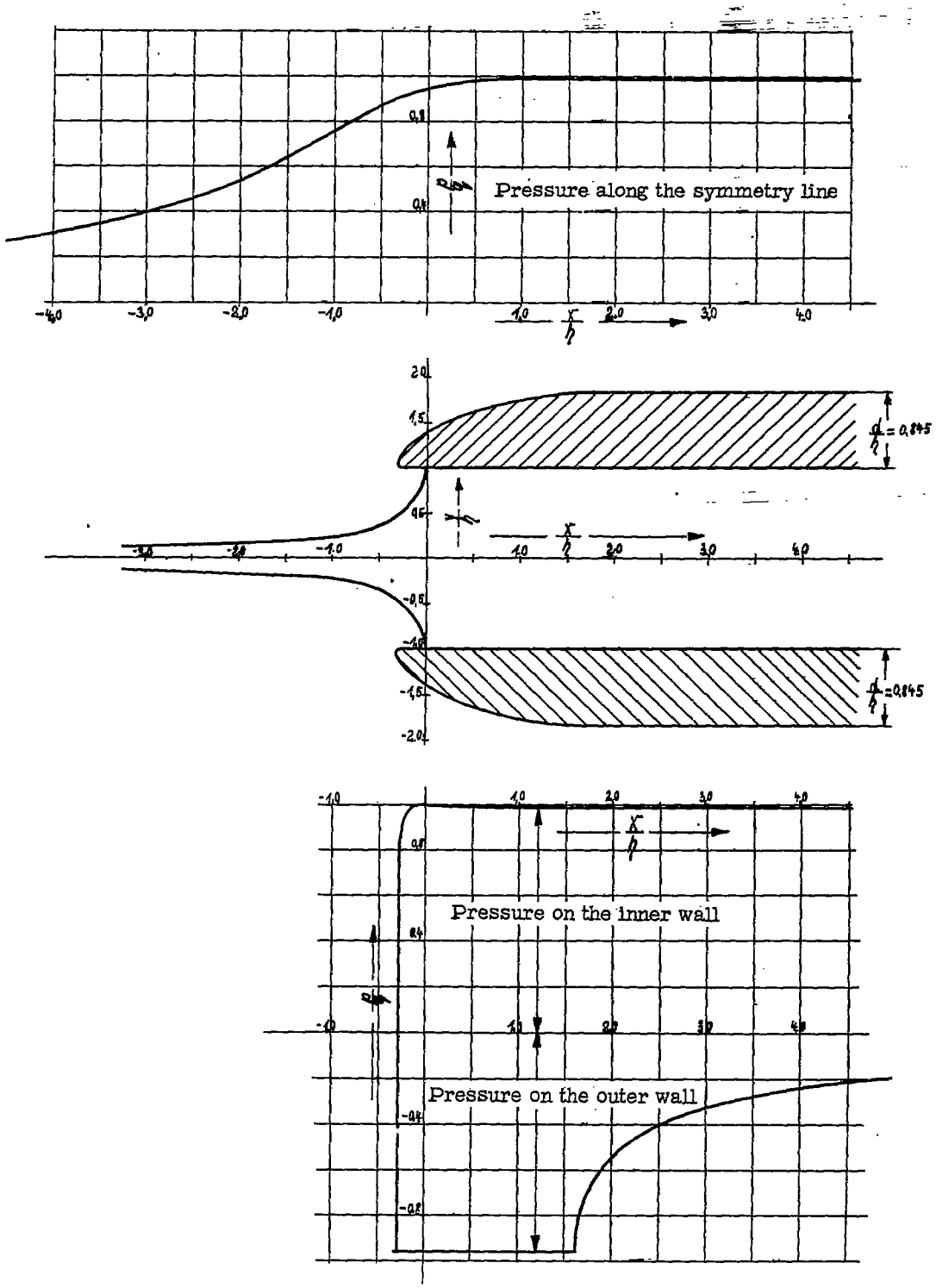

Figure 15.- Wall contours, stream lines, and pressure distributions of the simplest symmetrical inlet with external compression for $w_{max}/w_\infty = 1.4$ and $w_i/w_\infty = 0.1$.

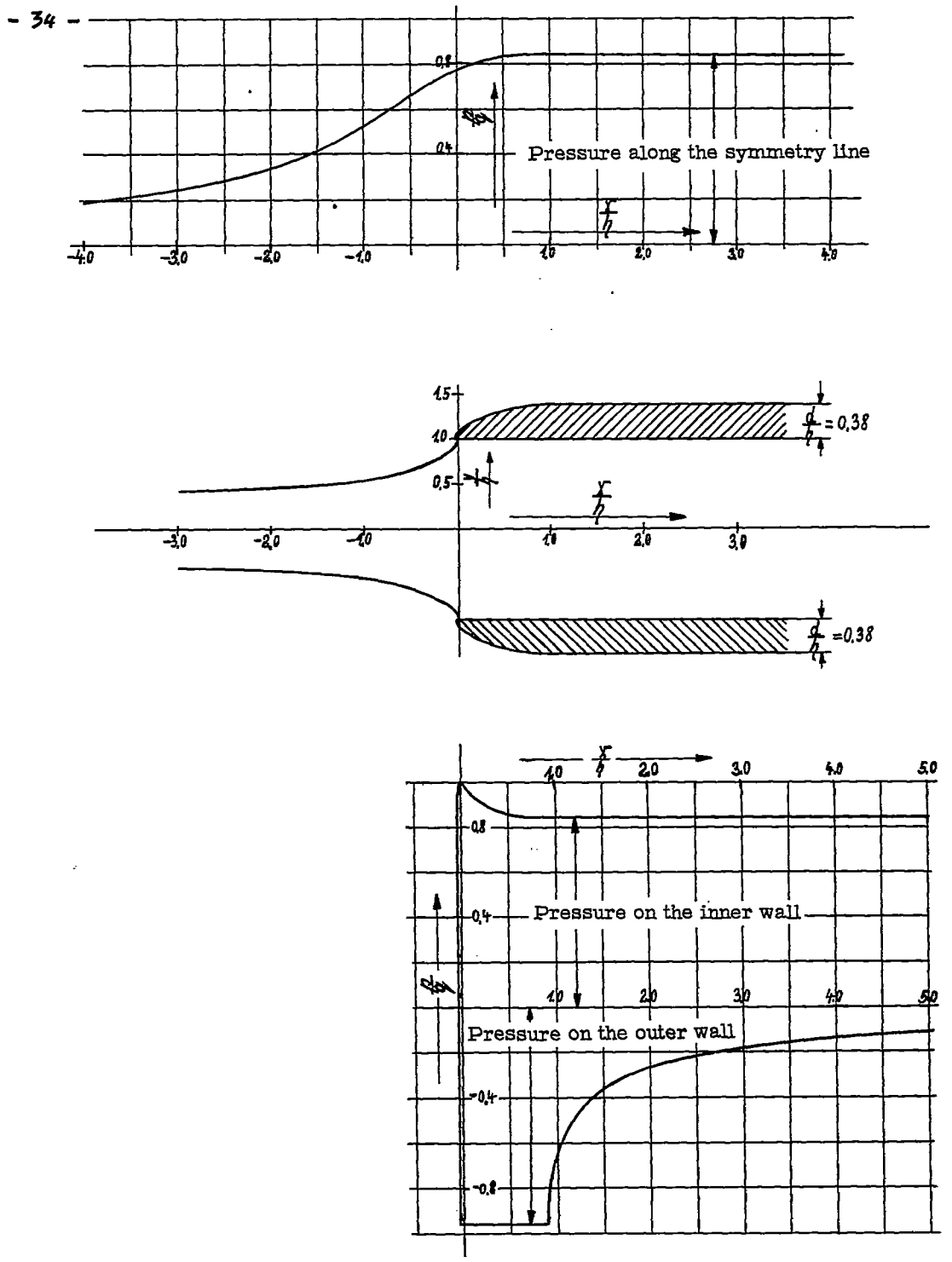

Figure 16.- Wall contours, stream lines, and pressure distributions of the simplest symmetrical inlet with external compression for $w_{max}/w_\infty = 1.4$ and $w_i/w_\infty = 0.4$.

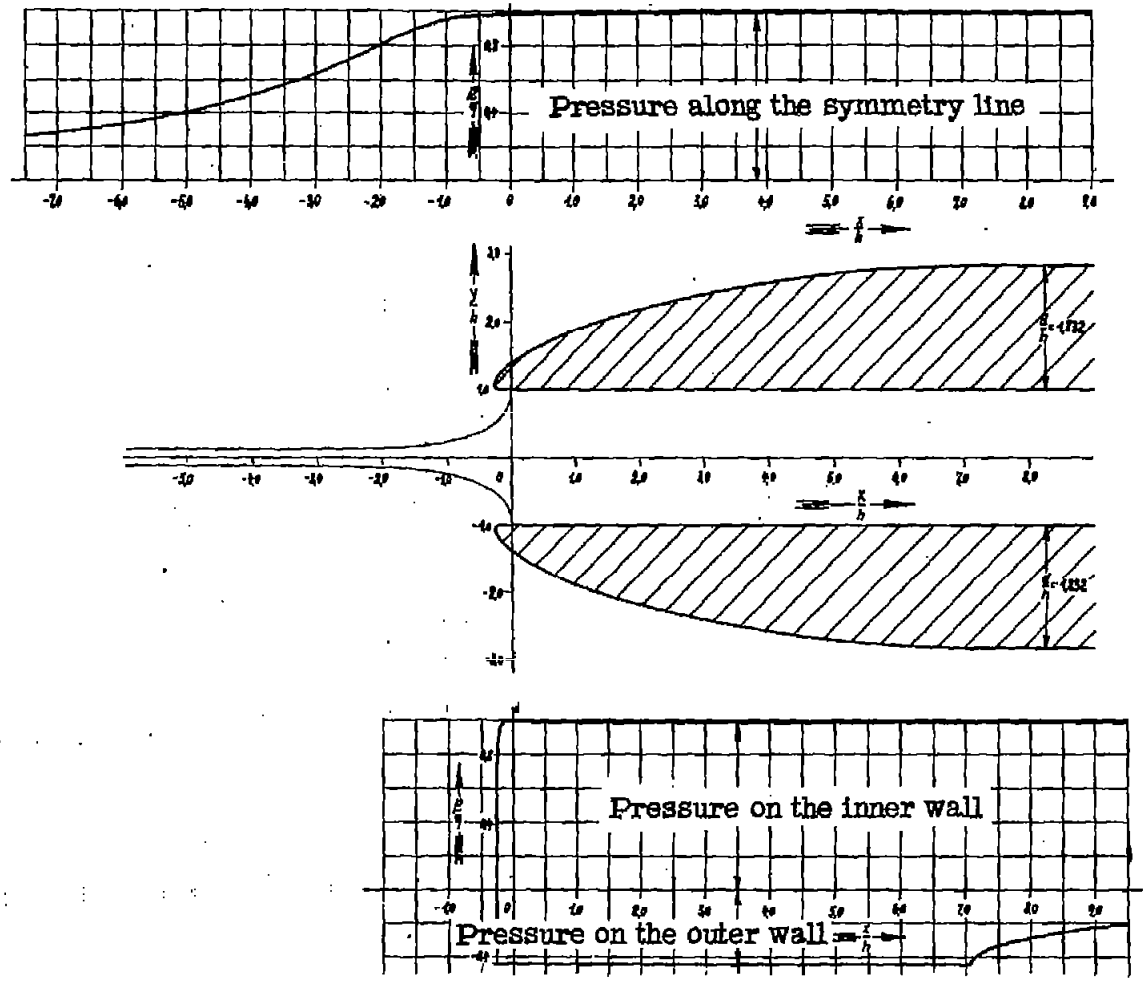

Figure 17.- Wall contours, stream lines, and pressure distributions of the simplest symmetrical inlet with external compression for $w_{max}/w_{\infty} = 1.2$ and $w_i/w_{\infty} = 0.1$.

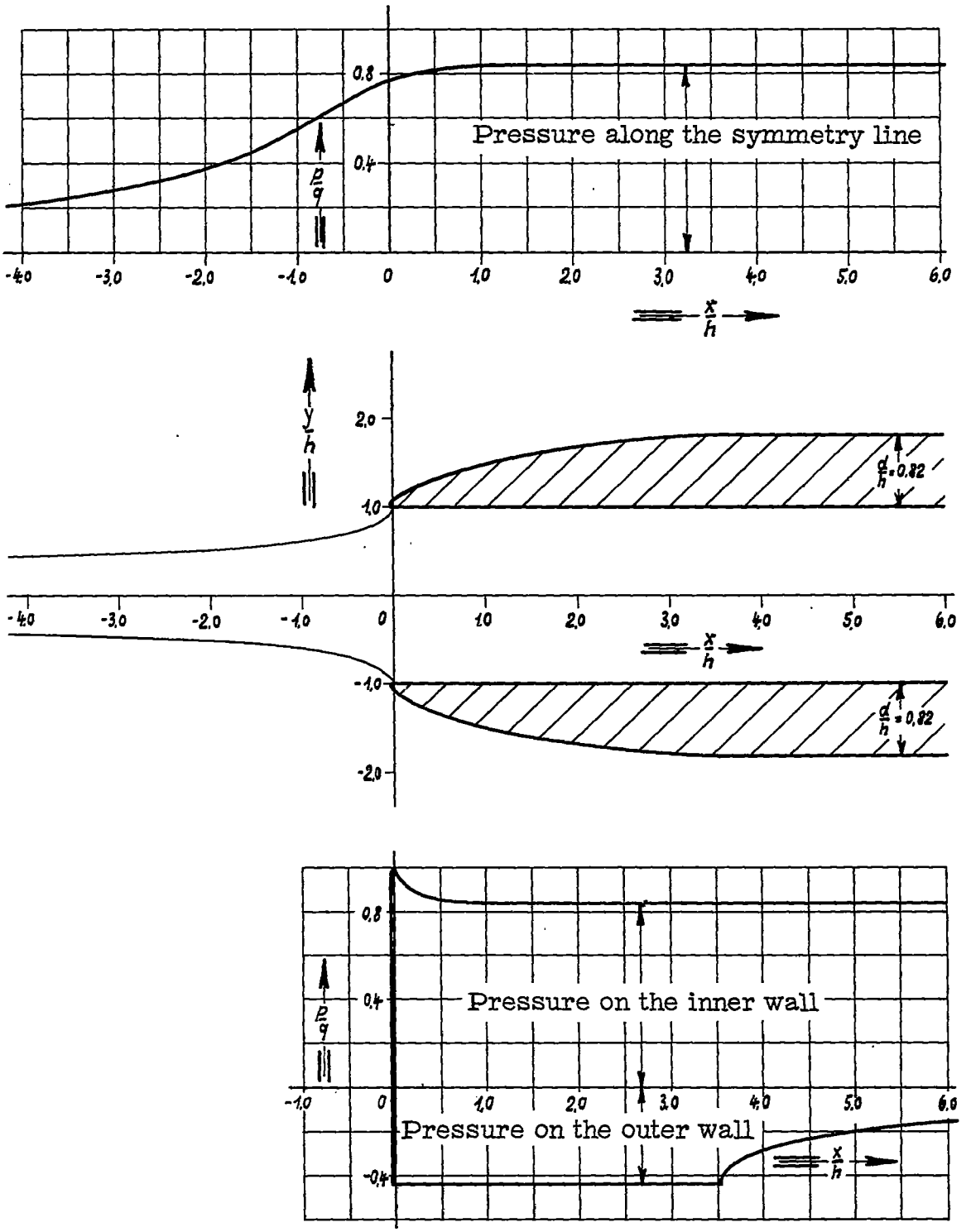

Figure 18.- Wall contours, stream lines, and pressure distributions of the simplest symmetrical inlet with external compression for $w_{max}/w_{\infty} = 1.2$ and $w_i/w_{\infty} = 0.4$ (Reviewer's note: This value was erroneously given as 0.1 in the original German version of this report.).

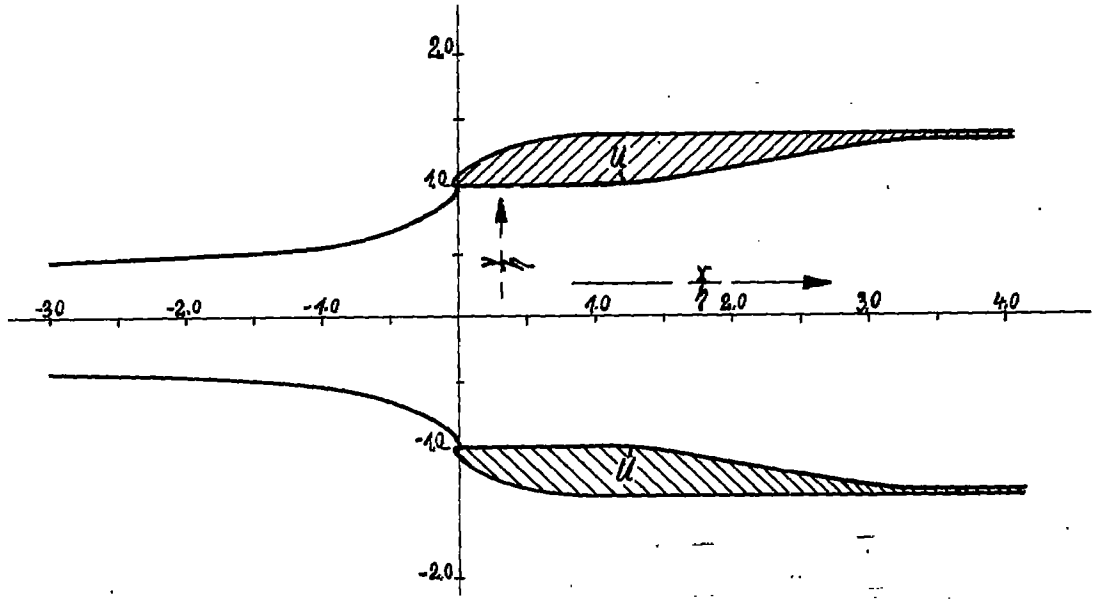

Figure 19.- External-compression inlet with wall thickness reduced from the inside. Starting from the external-compression inlet for $w_i/w_\infty = 0.4$, $w_{max}/w_\infty = 1.4$, one may thus obtain an external-compression inlet for $w_i/w_\infty = 0.3$, $w_{max}/w_\infty = 1.4$ without having to increase the maximum wall thickness.

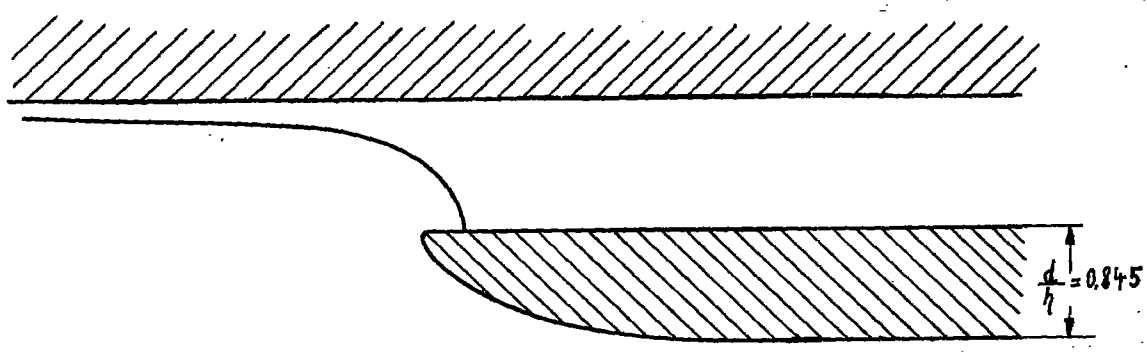

Figure 20.- Inlet with external compression for $w_i/w_\infty = 0.1$, $w_{max}/w_\infty = 1.4$, derived from figure 15. The symmetry stream line of figure 15 was made the solid wall.

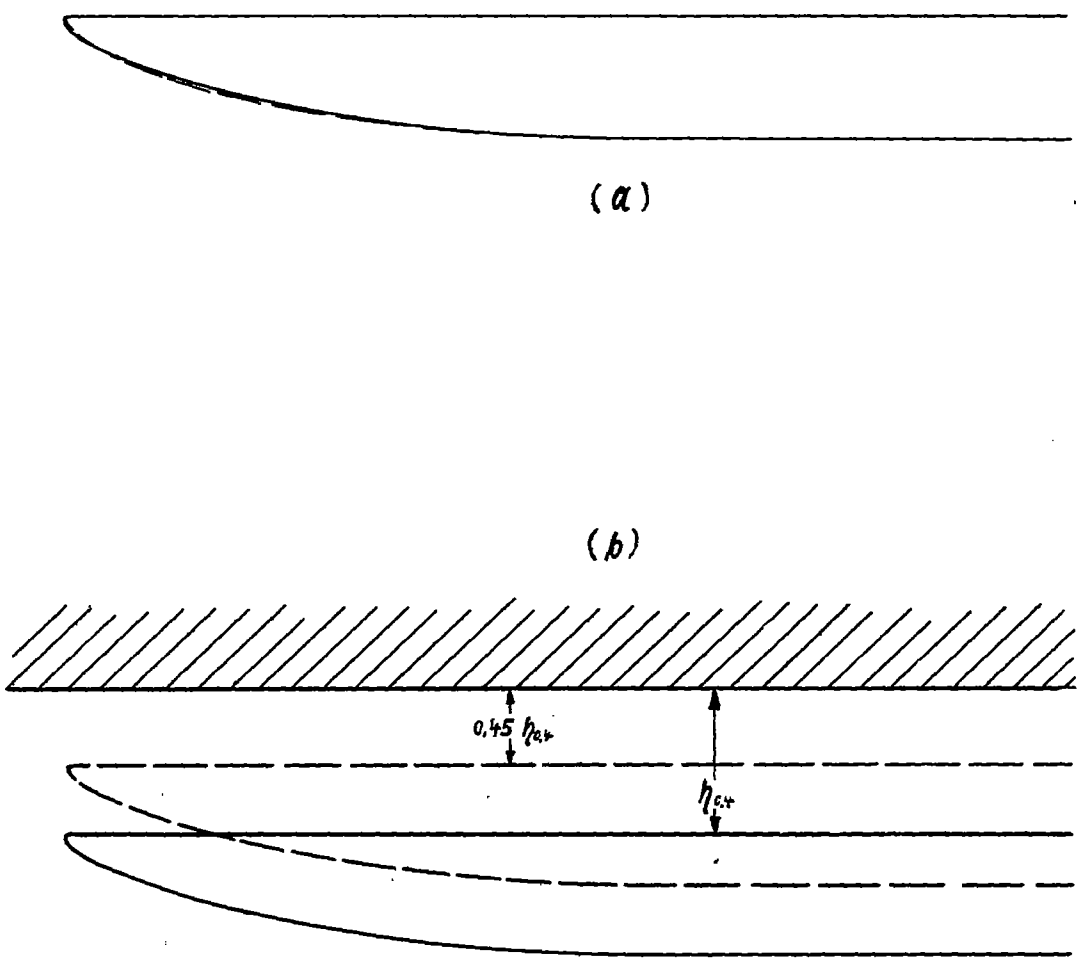

Figure 21.- Retractable inlet with external compression. In (a) the contour of the external-compression inlet for $w_i/w_\infty = 0.4$ and $w_{max}/w_\infty = 1.2$ and the contour of the external-compression inlet for $w_i/w_\infty = 0.1$ and $w_{max}/w_\infty = 1.2$, scaled to the same wall thickness, are plotted on top of each other. In (b) the positions of the retractable lower wall are represented for $w_i/w_\infty = 0.4$ (solid line) and for $w_i/w_\infty = 0.1$ (dashed line).

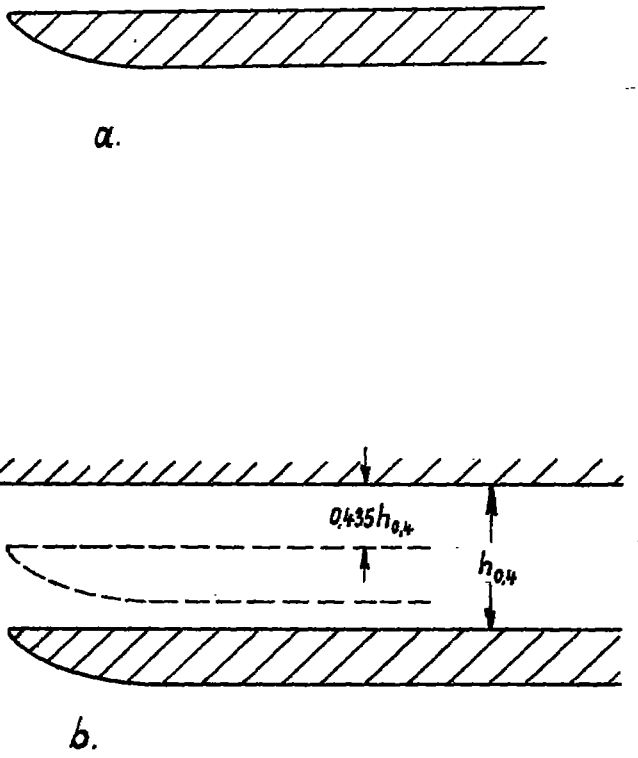

Figure 22.- Retractable inlet with external compression. In (a) the contour of the external-compression inlet for $w_i/w_\infty = 0.4$, $w_{max}/w_\infty = 1.4$ and the contour of the external-compression inlet for $w_i/w_\infty = 0.1$ and $w_{max}/w_\infty = 1.4$ scaled to the same wall thickness are plotted on top of each other. A difference can no longer be represented. In (b) the positions of the retractable lower wall are represented for $w_i/w_\infty = 0.4$ (solid line) and for $w_i/w_\infty = 0.1$ (dashed line).

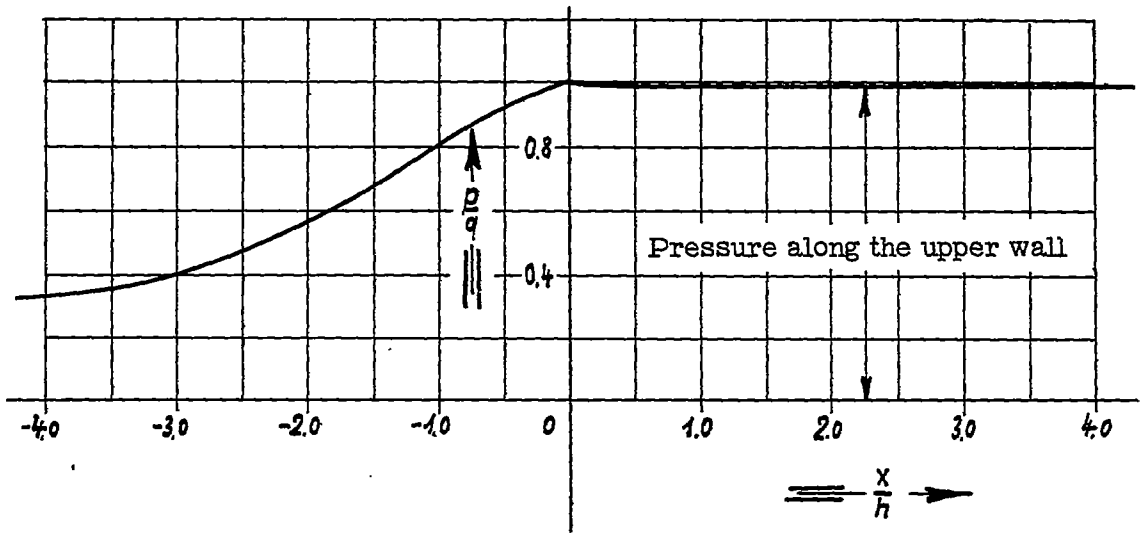

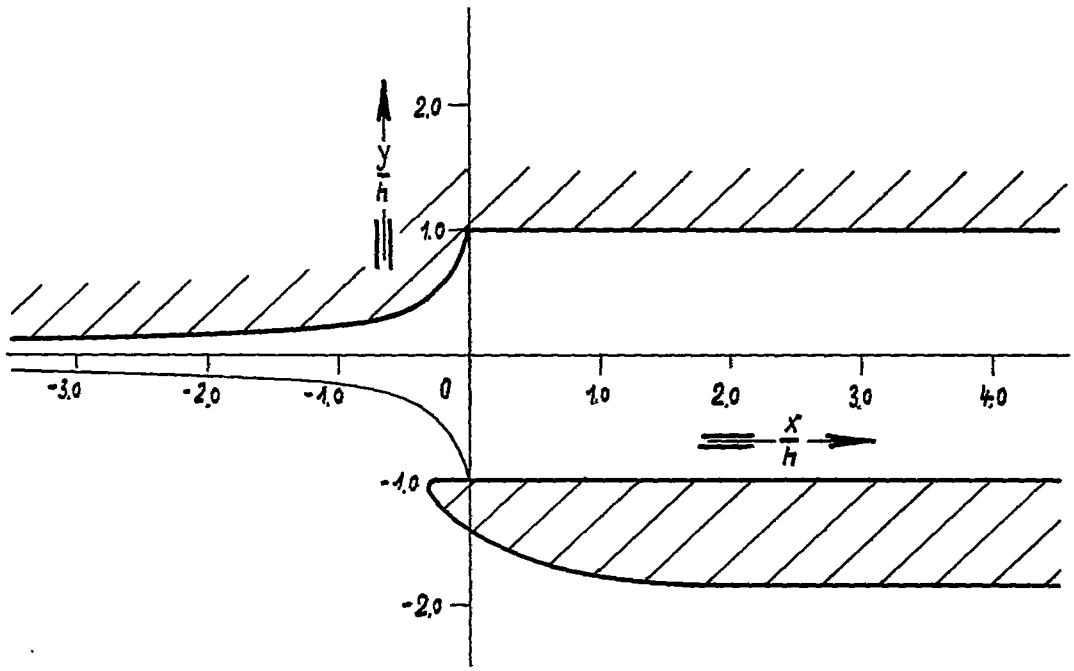

Figure 23.- With the stagnation-point stream line assumed as solid boundary, one obtains the most unsymmetrical external-compression inlet to be derived from the symmetrical one. ($w_i/w_\infty = 0.1$, $w_{max}/w_\infty = 1.4$).

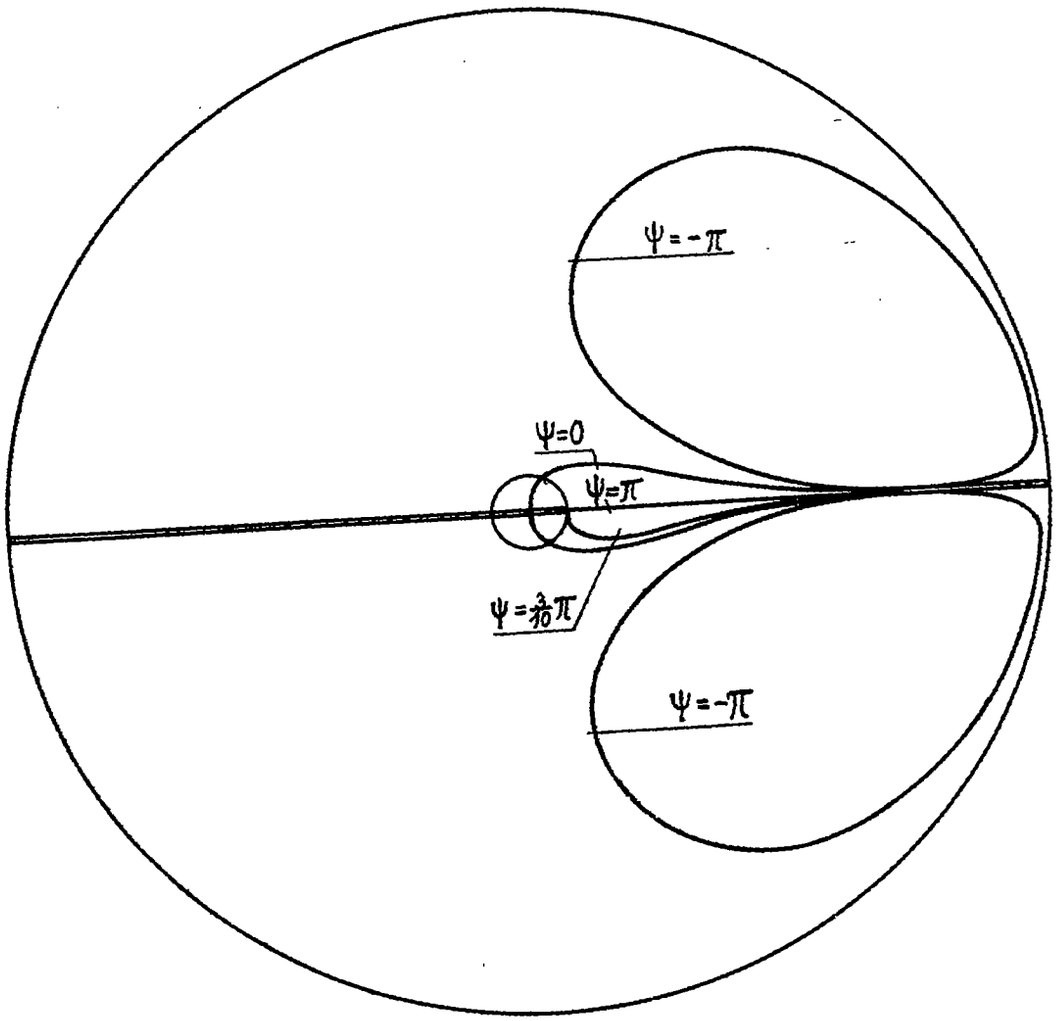

Figure 24.- In the hodograph for $w_i/w_\infty = 0.1$, $w_{max}/w_\infty = 1.4$, the stream line $\psi = 3\pi/10$ barely satisfies the condition that it must lie outside of a circle of the radius w_i/w_∞ around the zero point.

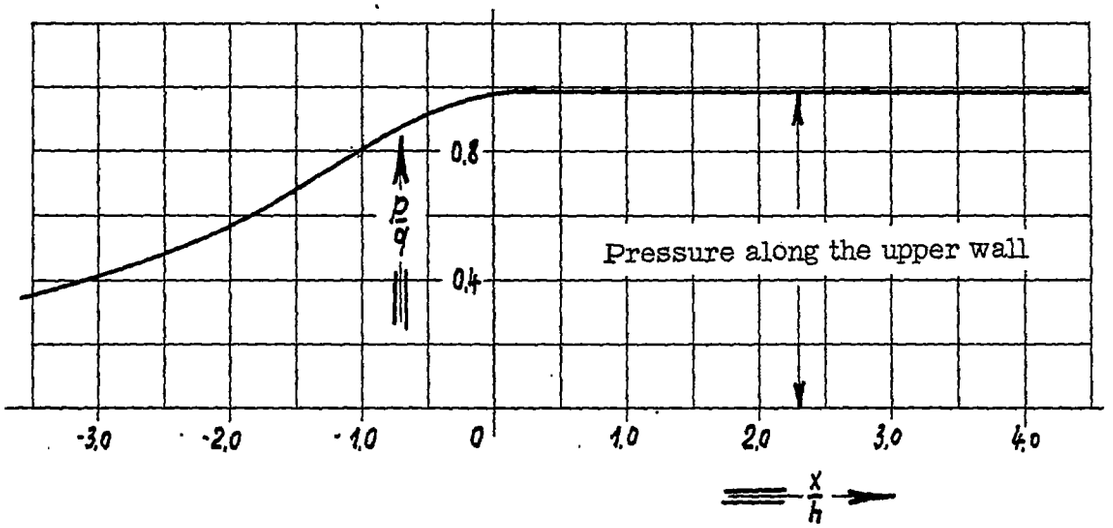

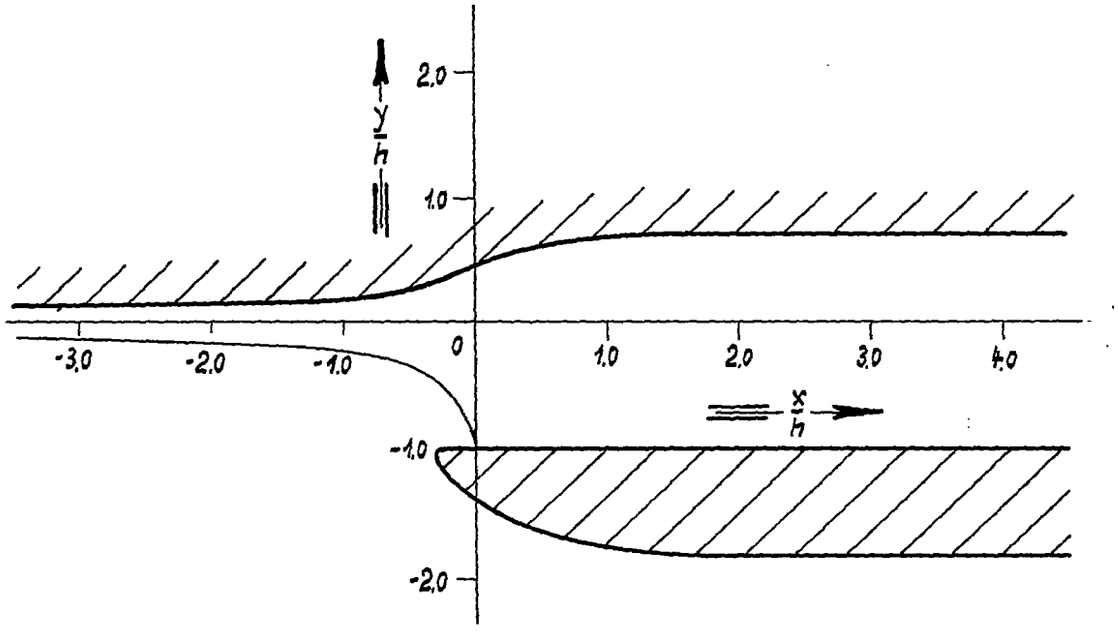

Figure 25.- If the stream line $\psi = 3\pi/10$ (see fig. 24) is made the solid wall, the pressure increases along this wall continuously and monotonically up to its end value p_i. ($w_i/w_\infty = 0.1$, $w_{max}/w_\infty = 1.4$).

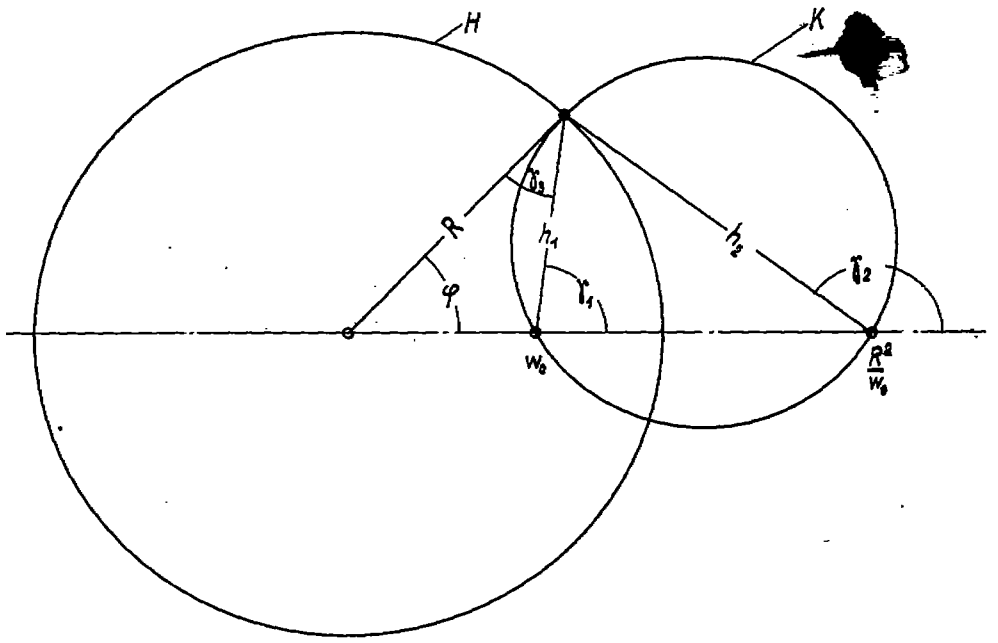

Figure 26.- As proof of the auxiliary theorems concerning points reflected on the circle.

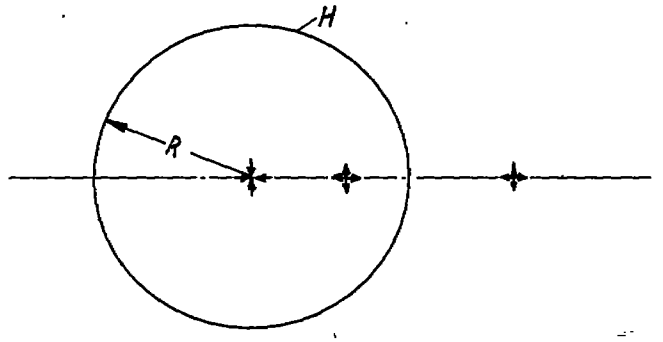

Figure 27.- Scheme of singularities for the derivation of the source potential within the circle.

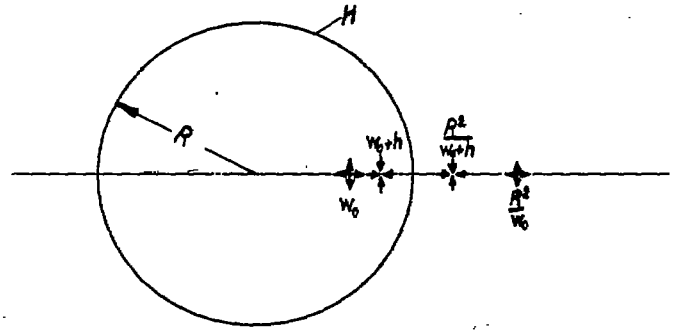

Figure 28.- Scheme of singularities for the derivation of the doublet potential within the circle.